



# 1 Geothermal heat flow in Antarctica: current and future 2 directions


3 Alex Burton-Johnson<sup>1</sup>, Ricarda Dziadek<sup>2</sup>, and Carlos Martin<sup>1</sup>

4 <sup>1</sup>British Antarctic Survey, High Cross, Madingley Road, Cambridge, CB3 0ET, UK

5 <sup>2</sup>Alfred Wegener Institute - Helmholtz Centre for Polar and Marine Research, Am Alten Hafen, Bremerhaven,  
6 Germany

7 *Correspondence to:* Alex Burton-Johnson (alerto@bas.ac.uk)

## 8 1. Abstract

9 Antarctic geothermal heat flow (GHF) affects the temperature of the ice sheet, determining its ability to slide and  
10 internally deform, as well as the behaviour of the continental crust. However, GHF remains poorly constrained,  
11 with few and sparse local, borehole-derived estimates, and large discrepancies in the magnitude and distribution  
12 of existing continent-scale estimates from geophysical models. We review the methods to ~~extract~~  GHF, compile  
13 borehole and probe-derived estimates from measured temperature profiles, and recommend the following future  
14 directions: 1) Obtain more borehole-derived estimates from the subglacial bedrock and englacial temperature  
15 profiles. 2) Estimate GHF beneath the interior of the East Antarctic Ice Sheet (the region most sensitive to GHF  
16 variation) via long-wavelength microwave emissivity. 3) Estimate GHF from inverse glaciological modelling,  
17 constrained by evidence for basal melting. 4) Revise geophysically-derived GHF estimates using a combination  
18 of Curie depth, seismic, and thermal isostasy models. 5) Integrate in these geophysical approaches a more accurate  
19 model of the structure and distribution of heat production elements within the crust, and considering  
20 heterogeneities in the underlying mantle. And 6) continue international interdisciplinary communication and data  
21 access.

22

# Summary of Comments on tc-2020-59\_BVL.pdf

---

## Page: 1

---



Number: 1      Author: brice      Subject: Sticky Note      Date: 13/04/2020 11:20:51

---

This might seem to be a picky comment but it is important to be precise. I would suggest to use "flux" than "flow": heat flow should be reserved for the movement of material while heat flux is a transport of a quantity of energy over time. As in this paper you focus more on the GHF beneath the Ice Sheet (bedrock surface), I would use "flux". Otherwise can you explain the use of "flow" ?



Number: 2      Author: brice      Subject: Inserted Text      Date: 13/04/2020 11:20:59

---

"estimate" (extract sounds like by effort or force)



## 23 1. Introduction

24 The Antarctic ice sheet is the world's largest potential driver of sea level rise, and accurately modelling its  
 25 dynamics relies, amongst others, on constraining conditions at the ice-bedrock interface. Measuring these basal  
 26 conditions is inherently challenging and, of all the parameters affecting ice sheet dynamics, subglacial geothermal  
 27 heat flow (GHF) is the least constrained (Larour et al., 2012; Llubes et al., 2006). Despite this uncertainty, GHF  
 28 affects (1) ice temperature and, as a consequence, ice mechanical properties (rheology), (2) basal melting and  
 29 sliding, and (3) the development of unconsolidated water-saturated sediments; all of which can promote ice flow  
 30 (Greve and Hutter, 1995; Larour et al., 2012; Siegert, 2000; Winsborrow et al., 2010). Beyond ice dynamics, our  
 31 knowledge of GHF allows us to model <sup>1</sup> basal melt rates in our exploration for old ice core climate records,  
 32 constrain models of glacial isostatic adjustment (GIA), and inform on the geological and tectonic development of  
 33 Antarctica.

34 In recognition of the ambiguity and importance of Antarctic GHF, an increasing number of studies in geology,  
 35 geophysics, and glaciology have sought to constrain this parameter, with a developing dedicated multinational  
 36 interdisciplinary community (Burton-Johnson et al., 2019; Halpin and Reading, 2018). However, with an  
 37 expanding research base and a requirement for multidisciplinary science, the necessity for a multidisciplinary  
 38 review of current approaches and future directions was highlighted by the GHF sub-group of SERCE (Solid Earth  
 39 Response and influence on Cryospheric Evolution) and the Scientific Committee on Antarctic Research (SCAR)  
 40 (Burton-Johnson et al., 2019).

### 41 1.1. What is geothermal heat flow (GHF)? <sup>2</sup>

42 GHF describes the transport of heat energy from the interior of the Earth to the surface (Gutenberg, 1959; Pollack  
 43 et al., 1993). This heat originates from two primary sources: 1) The primordial heat remaining from the formation  
 44 of the Earth, when the kinetic energy of celestial collisions was transformed into heat energy; and 2) the  
 45 radioactive decay of heat-producing elements (HPEs) and their isotopes; 98% of which is derived from Uranium,  
 46 Thorium, and Potassium (Beardmore and Cull, 2001; Lowrie, 2007). The HPEs are incompatible with the mineral  
 47 structures of the mantle, so are concentrated into the crust (Boden, 2016; McDonough and Sun, 1995). Other  
 48 sources of possible contributions to GHF are: 1) geoneutrino emission from the mantle (Huang et al., 2013;  
 49 Korenaga, 2011), and 2) gravitational pressure (Elbeze, 2013; Morgan et al., 2016).

50 The estimated average heat flow of continental crust is  $67.1 \text{ mW m}^{-2}$ , whilst for oceanic crust it is  $78.8 \text{ mW m}^{-2}$   
 51 (Lucazeau, 2019; although estimates vary according to sampling strategy and the number of observations). The  
 52 difference between continental and oceanic heat flow reflects the lower thickness of oceanic crust, with hot mantle  
 53 rocks at comparatively shallow depths. Continental GHF varies significantly, primarily in response to variations  
 54 in crustal heat production, age, composition, tectonic history, and thickness of crust and mantle (Mareschal and  
 55 Jaupart, 2013). This results from the geological complexity of composite continental crust compared with oceanic  
 56 crust. GHF is generally lower in stable crust away from convergent and divergent continental margins and rift  
 57 basins, and higher in these magmatically active provinces (Lucazeau, 2019; Pollack et al., 1993). On a broad  
 58 regional scale, continental GHF correlates negatively with age, allowing first order empirical estimation of  
 59 Antarctic GHF based on its range of crustal ages (Fig. 1; Llubes et al., 2006; Sclater et al., 1980). However,  
 60 Antarctic crustal heat production estimates show high variability across sampled age ranges (Gard et al., 2019),

## Page: 2



---

Number: 1      Author: brice      Subject: Inserted Text      Date: 13/04/2020 11:21:24

---

present and



---

Number: 2      Author: brice      Subject: Sticky Note      Date: 13/04/2020 11:21:30

---

See comment on the Title



with lithology and tectonic setting being important controls on the heat production distribution (Carson et al., 2014; Halpin et al., 2019).

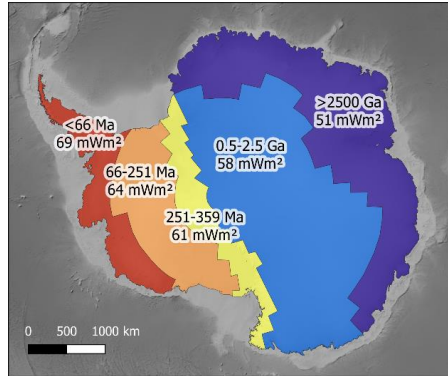


**Fig. 1. Empirical estimation of GHF based on generalised Antarctic crustal ages and mean global GHF values of continental crust of similar age (adapted from Llubes et al., 2006). Basemap bathymetry from ETOPO1 (Amante and Eakins, 2009).**

The rate of heat flow,  $Q$ , can be approximated by the Fourier's Law (Baron Fourier, 1822). In the simple model of a homogenous material with a constant thermal gradient, this equates to:

$$Q = -\kappa \partial T / \partial z$$

(1)

Where  $Q$  has the units  $\text{mW m}^{-2}$  (i.e. power per unit area);  $T$  is the temperature (K),  $z$  is the vertical distance (m); and  $\kappa$  is the thermal conductivity of the material ( $\text{mW m}^{-1} \text{K}^{-1}$ ). When considering the basal conditions of the Antarctic ice sheet, we are interested in the heat flow at bedrock surface. We also need to consider internal heat production,  $A$  ( $\mu\text{W m}^{-3}$ ). For a simple case of constant thermal conductivity and heat production, surface heat flow can be described by:

$$Q = \lambda_d$$

(2)

Where the integral is measured from the surface to a depth,  $d$  (Beardsmore and Cull, 2001).

We would like to highlight here that most methods to estimate GHF derive it from the temperature gradient, as in Equations 1 and 2. However, these equations are a simplification, as temperature variation over time, surface topography, internal heat production, and variation in the properties of the material all affect the observed temperature gradient.

This page contains no comments



## 83 2. Motivation: What is the importance of GHF in Antarctica?

### 84 2.1. Glaciology

85 GHF strongly influences the <sup>1</sup> ice sheet temperature. As a consequence, it is a key contributor to basal meltwater  
 86 production, ice rheology, basal friction, <sup>2</sup> sliding velocity, and erosion (Fahnestock et al., 2001; Goelzer et al., 2017;  
 87 Hughes, 2009).

88 The heat budget at the base of an ice sheet can be described (Vieli et al., 2018):

$$89 Q_g + Q_s + Q_w + Q_p + Q_f + Q_c = 0$$









90 (3)

91 Where  $Q_g$  is the GHF,  $Q_s$  is the heat generated by sliding,  $Q_w$  is the heat generated by subglacial water flow,  $Q_p$   
 92 is the heat required to maintain the flowing water at pressure melting point, and  $Q_f$  is the heat released by freezing  
 93 or used by melting; and  $Q_c$  is the heat conducted away in the ice towards the ice surface. Of the positive  
 94 contributions to basal heat, that generated by sliding ( $Q_s$ ) can be orders of magnitude greater than that from GHF  
 95 ( $Q_g$ ), but in slow flowing areas  $Q_s$  is negligible and GHF plays a key role in the heat budget (Larour et al., 2012;  
 96 Pittard et al., 2016a).

97 To illustrate this point, Llubes et al. (2006) modelled a  $20 \text{ mW m}^{-2}$  increase in GHF across the Antarctic continent  
 98 (from uniform values of  $40$  to  $60 \text{ mW m}^{-2}$ ). This resulted in a  $6^\circ\text{C}$  increase in the mean basal temperature, <sup>3</sup>  
 99  ~~$7^\circ\text{C}$  to  $-13^\circ\text{C}$~~ , <sup>4</sup> this variation directly affects the basal melt rates, with a uniform  $40 \text{ mW m}^{-2}$  generating  $6.7 \text{ km}^3$   
 100  $\text{yr}^{-1}$  of basal melting across Antarctica, whilst  $60 \text{ mW m}^{-2}$  would generate  $18 \text{ km}^3 \text{ yr}^{-1}$ . However, unlike the GHF  
 101 values used, the resultant basal temperature variation is non <sup>5</sup> uniform: Whilst the two heat flow models produce  
 102 only a few  $^\circ\text{C}$  difference in basal temperature near the coast, they generate up to  $15^\circ\text{C}$  difference in central East  
 103 Antarctica. This is because horizontal advection and frictional basal heating are negligible beneath the thick, slow  
 104 moving ice of East Antarctica, and surface temperatures have a reduced effect on basal conditions (Llubes et al.,  
 105 2006; Pollard et al., 2005). Also, in these regions of thick ice, the increased pressure brings the basal ice  
 106 temperature closer to its pressure melting point (PMP; Pollard et al., 2005). Variation in GHF thus determines  
 107 whether basal melting occurs, with a resultant effect on the basal friction and sliding of the ice sheet (Pollard et  
 108 al., 2005). In addition, the increased ice temperature makes it more susceptible to internal deformation, which also  
 109 enhances its ability to flow (Llubes et al., 2006). <sup>6</sup>

110 Even beneath the comparatively thinner ice of West Antarctica, the sensitivity of basal temperature to heat flow  
 111 is enhanced (Llubes et al., 2006). There is evidence that this region, dominated tectonically by the West Antarctic  
 112 Rift System (Jordan et al., 2020), exhibits very high values of basal heat flow and resultant basal melting  
 113 (Schroeder et al., 2014). Above  $85 \text{ mW m}^{-2}$ , the basal temperature of much of the West Antarctic Ice Sheet will  
 114 pass its pressure melting point (in agreement with radar evidence for extensive basal melting; Llubes et al., 2006;  
 115 Rémy and Legresy, 2004; Schroeder et al., 2014). Consequently, enhanced basal heat flow in West Antarctica can  
 116 have a large effect on its basal melt rates, although the thinner ice sheet in West Antarctica compared to East  
 117 Antarctica makes it more sensitive to surface parameters (accumulation and surface temperature; Llubes et al.,  
 118 2006).

## Page: 4

- 
-  Number: 1    Author: brice    Subject: Sticky Note    Date: 13/04/2020 11:21:50  
I would suggest to add somewhere that ice sheet temperature is also influenced by the ice thickness: as ice acts as an insulator, the greater the ice thickness, the warmer the ice at the base. This is counterbalanced by cold temperature advecting from the surface, itself influenced the accumulation rate.
- 
-  Number: 2    Author: brice    Subject: Inserted Text    Date: 06/04/2020 15:43:05  
whole
- 
-  Number: 3    Author: brice    Subject: Inserted Text    Date: 06/04/2020 15:43:59  
basal
- 
-  Number: 4    Author: brice    Subject: Cross-Out    Date: 06/04/2020 15:59:01
- 
-  Number: 5    Author: brice    Subject: Inserted Text    Date: 06/04/2020 15:58:43  
"increase" ==> from -13°C to 7°C
- 
-  Number: 6    Author: brice    Subject: Inserted Text    Date: 13/04/2020 11:23:23  
and expands the surface area of the bed at the pressure point from 16% to more than 50%.
- 
-  Number: 7    Author: brice    Subject: Cross-Out    Date: 06/04/2020 16:01:57
- 
-  Number: 8    Author: brice    Subject: Inserted Text    Date: 13/04/2020 11:23:44  
As you mention surface temperature in this paragraph, I suggest to add a sentence on surface accumulation which can have a strong influence on the basal conditions even in the interior of the ice sheet, and counteract the effect of the GHF (see Fig. 2 Van Liefferinge and Pattyn 2013)






In addition to enhancing basal melting and reducing basal friction, increased GHF enhances ice flow by increasing the englacial temperature and thus reducing the ice stiffness (Larour et al., 2012). Because the heat produced by basal friction and viscous deformation are orders of magnitude greater than from GHF in fast-flowing ice streams, this effect is only significant in upstream, slow-flowing areas (Larour et al., 2012). In these regions of thick, slow-flowing ice, even local high heat flow anomalies of insufficient heat for basal melting can result in the development of accelerated, channelised flow for hundreds of kilometres upstream and downstream of the GHF anomaly (Pittard et al., 2016a). Regions along ice divides and adjacent to ice streams are particularly sensitive to enhanced GHF (Pittard et al., 2016b).

Whilst the points above highlight the necessity of estimating Antarctic GHF, it is very important that the accuracy of these estimates can be verified. The impact of inaccurate GHF constraints on models of ice sheet dynamics have been shown by comparing GHF estimates for Greenland. Ice sheet modelling controlled by spatially variable GHF forcing reproduces the observed state to only a limited degree, and fails to reproduce either the topography or the low basal temperatures measured in southern Greenland (Rogozhina et al., 2012).<sup>1</sup> Instead, an unrealistic spatially uniform GHF forcing produces a considerably better fit. If the much larger Antarctic ice sheet is to be accurately modelled, the accuracy of the GHF estimates used must be well constrained by multiple independent methodologies, sensitivity tests, and comparison of different models.

Recently, there has been increasing interest in the exploration of suitable locations for coring Antarctica's oldest continuous ice record.<sup>2</sup> This problem requires accurate knowledge of GHF, as basal melt rates limit the maximum possible age of recoverable ice (Offringa et al., 2018).<sup>3</sup> Additionally, due to environmental concerns around possible drilling fluid contamination, frozen bed conditions are a prerequisite for deep coring operations.

## 2.2. Glacial Isostatic Adjustment (GIA)


The temperature of the lithosphere and upper mantle are important parameters for modelling the isostatic response to changes in the volume of the overlying ice sheet (i.e. glacial isostatic adjustment, GIA). This is because the (visco-)elastic properties of the lithosphere and mantle directly relate to its thermal properties (Chen et al., 2018; Kuchar and Milne, 2015). GIA is a critical component of the long-term evolution of ice sheets and could potentially stabilise retreating ice streams in submarine settings (Barletta et al., 2018; Kingslake et al., 2018). Of particular importance here is that the temperature-dependant viscosity that controls GIA can be modelled using surface heat flow estimates (van der Wal et al., 2013, 2015).

 Number: 1      Author: brice      Subject: Inserted Text      Date: 13/04/2020 11:24:25

---


You should also add the work of Rezvanbehbahani et al. (2017) : Rezvanbehbahani et al. (2017) use for the first time machine learning techniques to derive GHF from relevant geologic features (gravity measurements, magnetic anomaly) and GHF measurements (derived from crustal thickness, rock composition and active thermal feature).

S. Rezvanbehbahani, L. A. Stearns, A. Kadivar, J. D. Walker, and C. J. van der Veen. Predicting the geothermal heat flux in Greenland: a machine learning approach. Geophysical Research Letters, 2017. ISSN 1944-8007. doi: 10.1002/2017GL075661.

 Number: 2      Author: brice      Subject: Inserted Text      Date: 06/04/2020 16:33:34

---

Cit: Fischer 2013, Climate of the past paper. <https://www.clim-past.net/9/2489/2013/>

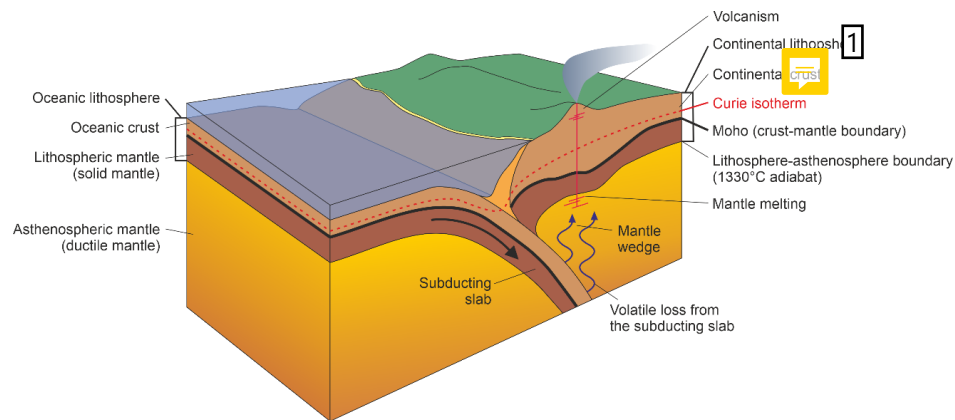
 Number: 3      Author: brice      Subject: Inserted Text      Date: 06/04/2020 16:12:44

---

Van Liefferinge and not Liefferinge



## 147 2.3. Geology and tectonics



148

149 **Fig. 2. Basic illustration of a subduction zone at a convergent margin between oceanic and continental lithosphere to**  
 150 **clarify the geological concepts and terms used in this paper.**

### 151 2.3.1. Mantle dynamics

152 Heat flow variation and its isostatic effects (i.e. the buoyancy control on crustal elevation, resulting from the  
 153 different densities of the dense mantle and less dense overlying crust) provide evidence for mantle dynamics  
 154 beneath a continent. For example, high heat flow anomalies have been proposed as evidence for sub-lithospheric  
 155 heating by present and past mantle plumes (regional hot spots of warm mantle upwelling beneath the lithosphere;  
 156 e.g. Courtney and White, 1986; Martos et al., 2018). The absence of enhanced heat flow where mantle ascent  
 157 is proposed has been used to argue against such processes (e.g. Stein and Stein, 2003). Also, because of the  
 158 relationship between surface heat flow and isostatic elevation, heat flow studies can reveal thermal or  
 159 compositional variation of the sub-continental mantle, as a reduction in its density can increase the isostatic  
 160 elevation of the surface topography (Hasterok and Gard, 2016).

### 161 2.3.2. Development of the lithosphere


162 The thermal properties of the lithosphere control its response to tectonic deformation (e.g. Sandiford and Hand,  
 163 1998), such as the development of crustal shear zones and earthquakes. The lithosphere's thermal properties also  
 164 affect the relative density of lithosphere and underlying mantle, and (as a result of this buoyancy effect) the  
 165 isostatic surface elevation. This in turn influences the heights of Antarctica's mountain ranges and the depths of  
 166 its sedimentary basins (McKenzie et al., 2005). For these reasons, understanding the continent's GHF will inform  
 167 on the development of many of Antarctica's largest tectonic features. For example, the lithospheric extension of  
 168 the West Antarctic Rift System, the prominent elevation of the Transantarctic Mountains, the deep topographic  
 169 depression of the Wilkes subglacial basin, and the extensive Palmer Land Shear Zone of the Antarctic Peninsula.

## 170 3. GHF estimates from measured temperature gradients


171 Having highlighted the importance of constraining Antarctica's GHF, the following sections discuss current  
 172 approaches to its estimation.

## Page: 6


---

 Number: 1    Author: brice    Subject: Sticky Note    Date: 10/04/2020 11:53:16  
Curie Point Depth (CPD as in section 4.1 L311)

---

 Number: 2    Author: brice    Subject: Sticky Note    Date: 10/04/2020 11:06:55  
I suggest to develop in one or two sentences the implications of the Antarctic Ice Sheet like in section 2.3.2

---

 Number: 3    Author: brice    Subject: Inserted Text    Date: 13/04/2020 11:25:39  
It is a simple suggestion but why not provide a table presenting all the methods used to estimate the GHF with the advantages and disadvantages, to have an overview of all the methods together. This sentence could be extended as well to give an overview of the section's content.



Local heat flow estimates can be derived by measuring the temperature at various depths below the surface (either in the bedrock, overlying sediments, or within the ice sheet) and deriving a temperature gradient. In Antarctica, GHF has been derived through temperature measurements from boreholes into the bedrock or into the ice sheet, and also from probes into unconsolidated sediments. It is important to recognise that these are “estimates” not “measurements” of GHF, particularly when using them to verify the accuracy of geophysical or inverse GHF estimates. This is because the measured thermal gradient can be affected by processes other than geothermal heat flow, including surface temperature variation and hydrothermal circulation. When evaluating a specific local estimate, its derivation, local geology, and other regional GHF estimates must be considered. Thermal gradients and surface heat flow may vary significantly over 10 km lateral spatial resolutions (Carson et al., 2014) with variations in geology (affecting heat production and conductivity; Carson et al., 2014; Hasterok and Chapman, 2011), hydrothermal circulation (affecting local heat convection and redistribution; Fisher and Harris, 2010), and topography (affecting heat diffusion pathways to the surface; Bullard, 1938; Lees, 1910).

### 3.1. Boreholes into bedrock

The thermal gradient can be determined by measuring the temperature variation at different depths in the crust. Away from Antarctica, these measurements are from boreholes (commonly those drilled for mineral or hydrocarbon exploration), mineshafts, caves, or other cavities. The temperature gradient of the crust’s uppermost 10-50 m is dominantly affected by downward conduction of the surface temperature rather than GHF. To address this, temperature measurements are made over the largest depth range possible (typically 100-1000 m).

Borehole temperature measurements are made using wire-line temperature probes, with a thermistor at the leading tip and measurements made progressively downwards to minimise disturbance of the borehole fluids prior to temperature measurement. The temperature is measured from the bore fluid, not the surrounding rock, so an important consideration is the need for thermal equilibration of the wall rock and the borehole fluids following drilling and prior to measurement. In addition, the heat produced during drilling needs to be dissipated from the borehole. As a guide, 10-20 times the drilling time is required before a borehole is equilibrated to within instrument accuracy (Bullard, 1947; Jaeger, 1956), although observations show that after 3 times the drilling time, borehole fluids are within 0.05°C of equilibrium values (Lachenbruch and Brewer, 1959). For the low water flows used in small-core (<4 cm diameter) diamond drilling (compared with wider core diameter rotary drilling) measurements can be taken about two days after drilling cessation, except from the upper and lowermost ~20 % of the borehole (Jaeger, 1961, 1965). As an example, drilling of the multiple Cape Roberts Project boreholes averaged 16-31 m day<sup>-1</sup> (Talalay and Pyne, 2017).

Depth below the bedrock surface must be considered when taking borehole temperature measurements. Where terrestrial bedrock is exposed, atmospheric temperature and seasonal variation perturbs the thermal gradient in the upper >100 m of the crust. In Antarctica, temperatures from Hole 3 of the Dry Valley Drilling Project provided estimates of “equilibrium” gradient only when deeper than 90 m (Decker, 1974; Decker et al., 1975; Pruss et al., 1974). It may be possible to compensate for seasonal variation in shallower boreholes using long-term observations of the temperature gradient (>1 year), although the previous attempt (from a 7.6 m borehole at McMurdo Station; Risk and Hochstein, 1974) derived an anomalously high GHF estimate (164 mW m<sup>-2</sup>, compared to 66 mW m<sup>-2</sup> from a 260 m deep borehole; Decker and Bucher, 1982).





211 Subglacial bedrock is not exposed to atmospheric temperature variation, so the geothermal gradient can be  
 212 measured from shallower depths. However, it is affected by heat derived from the overlying ice sheet: internal  
 213 and basal frictional shear heating from the ice sheet, heat advection, basal water, and seasonal temperature  
 214 variation (e.g. Ritz, 1987). In the absence of a deep, borehole-derived, subglacial bedrock temperature profile, the  
 215 depth required to accurately measure the unperturbed geothermal temperature gradient is currently unknown.  
 216 Thermal diffusion modelling over timescales of low frequency climate variation may constrain this.<sup>1</sup>

## 217 **2. Ice boreholes**

218 Subglacial GHF can be estimated from the temperature gradient from boreholes into the ice sheet (e.g. Engelhardt,  
 219 2004; Fudge et al., 2019; Nicholls and Paren, 1993). This requires that there is no additional heating from basal  
 220 shear or horizontal advection, and that ice sheet has been unequivocally frozen to the bed for long enough that the  
 221 bedrock and overlying ice sheet have thermally equilibrated. To meet this requirement, the temperature profile is  
 222 best measured from cores into the summits of ice domes where the ice sheet is stationary (Engelhardt, 2004). As  
 223 applies to bedrock boreholes, a delay between drilling and temperature measurement is required for the thermal  
 224 disturbance from the drilling to dissipate. For hot-water drilling, this can take 2 years (Barrett et al., 2009;  
 225 Engelhardt, 2004). The temperature profile is typically measured using thermistors, recording the temperature  
 226 through changes in resistivity to electrical currents. Either a string of thermistors is deployed into the borehole  
 227 prior to freezing, and the temperature recorded over time, or the hole can be kept open with drill fluid and  
 228 downhole temperature measured with a moving thermistor. More recently, temperature has been recorded also  
 229 using distributed temperature systems (DTS).<sup>3</sup> The temperature is derived from the travel time of a laser beam  
 230 within an optical fibre. All of these methods require thermal equilibration.

231 Once the englacial temperature profile is obtained, GHF estimation can be achieved through three methods.  
 232 Firstly, if the borehole reaches the ice-bedrock interface, and the bedrock and overlying ice are in thermal  
 233 equilibrium, then the GHF can be estimated in the same way as for bedrock boreholes (e.g. Engelhardt, 2004).  
 234 That is, using the temperature gradient in the ice near the ice-bedrock interface but using the thermal conductivity  
 235 of ice rather than rock (Equation 1). Secondly, rather than measuring a temperature profile above the bed, the  
 236 basal temperature at the ice-bedrock interface can be measured, and temperature modelled through time to  
 237 constrain the required GHF (e.g. Fudge et al., 2019). Thirdly, if the borehole doesn't reach bedrock, and similarly  
 238 to the previous method, a thermal model is required to constrain GHF (e.g. Zagorodnov et al., 2012). In the  
 239 methods where modelling is required, the variables are modified within constraints determined for the location  
 240 until the modelled temperature profile best fits the measurements (Fig. 3), and the modelled temperature gradient  
 241 within the bedrock used for GHF calculation.

## Page: 8

---



Number: 1      Author: brice      Subject: Inserted Text      Date: 13/04/2020 11:26:05

---

In the xlsx supplementary material, I guess that in the row "method", borehole means "Boreholes into bedrock" ? If yes can you provide the exhaustive (or estimation) of the number of boreholes into bedrock in Antarctica and cite the SOM



Number: 2      Author: brice      Subject: Underline      Date: 13/04/2020 11:26:38

---

A key point that is not explained here, is that, when the base of the ice sheet is at the pressure melting point (presence of water), the GHF estimate is a minimum GHF estimate, which means that the GHF can be higher! See also section 5, 5.1



Number: 3      Author: brice      Subject: Inserted Text      Date: 10/04/2020 11:26:41

---

add citation



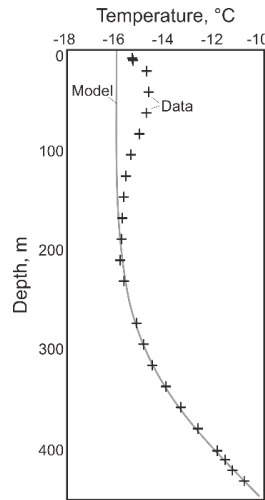


**Fig. 3. An example of temperature measurements (crosses) and steady state model (grey line) from which GHF can be estimated. Adapted from Zagorodnov et al. (2012) for the LARISSA Site Beta ice borehole temperature profile from the Bruce Plateau, Antarctic Peninsula. Note that it is the deeper temperature gradient that is modelled rather than the shallower temperature variation.**

GHF can be estimated from boreholes that do not reach the bedrock providing that the temperature profile is obtained below the penetration depth (or skin depth,  $\delta$ ) of surface temperature variation into the ice sheet. This depth is defined by the circular frequency of the variation ( $\omega$ ), and the thermal diffusivity of the material ( $k$ ) according to the Equation 4 (Fig. 4; Carslaw and Jaeger, 1959; Wangen, 2010).

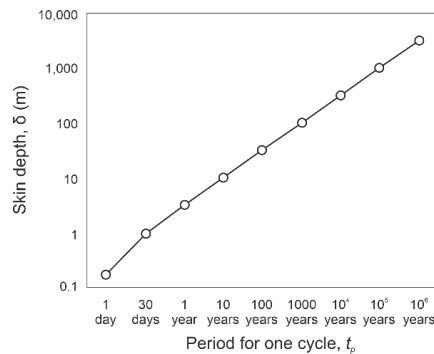
$$\delta = \sqrt{(2k/\omega)}$$

(4)

Where circular frequency ( $\omega$ ) is defined by Equation 5, where  $t_p$  is the time for one period (or cycle) of the temperature variation (Wangen, 2010).

$$\omega = 2\pi/t_p$$

(5)



This page contains no comments



258 **Fig. 4. Relationship between skin depth and periodicity of temperature variation through a material of thermal**  
 259 **diffusivity,  $k$ , of  $10^{-6} \text{ m}^2 \text{ s}^{-1}$ . This diffusivity is comparable to ice at  $-10^\circ\text{C}$  (James, 1968), or average values of a range**  
 260 **of rock types at  $-50^\circ\text{C}$  (Vosteen and Schellschmidt, 2003), and increases with decreasing temperature for both**  
 261 **materials.**

262 The deepest significant perturbations of the englacial temperature profile are from glacial-interglacial cycles, and  
 263 GHF is best estimated from the englacial temperature profile below the depth at which this effect becomes  
 264 negligible. In Greenland, this is the bottom 20 % of the ice sheet, but in areas of low-accumulation in Antarctica  
 265 this can extend to much shallower depths. With sufficiently accurate temperature measurements, the full  
 266 temperature profile of the ice sheet and the subglacial GHF may be estimated from boreholes penetrating only the  
 267 upper 600 m or 20 % of the total ice sheet thickness (Hindmarsh and Ritz, 2012; Mulvaney et al., 2019; Rix et al.,  
 268 2019).

269 However, poorly-constrained thermal effects within the ice sheet propagate uncertainties in GHF estimates from  
 270 ice sheet boreholes (Cuffey and Paterson, 2010, Chapter 9). This is a particular problem if there is any ambiguity  
 271 as to whether the ice sheet is frozen to the bed. The englacial temperature profile depends on heat sources at the  
 272 surface, base, and within the ice (i.e. internal deformation-derived frictional heating). Heat sources that act at the  
 273 base of the ice, such as frictional heating by basal motion, are impossible to differentiate from GHF.

### 274 3.3. Marine and onshore unconsolidated sediments

275 Shallow ( $< \sim 10 \text{ m}$ ) temperature gradients in unconsolidated sediments can be recorded using gravity-driven probes  
 276 rather than drilled boreholes. They carry multiple thermistors along the length of the probe that provide a  
 277 temperature profile. These measurements can be taken from unconsolidated sediments offshore (e.g. Dziadek et  
 278 al., 2019, 2017), in subglacial lakes (Fisher et al., 2015) or below ice shelves (Begeman et al., 2017).

279 As applies to borehole measurements, temperature gradients in unconsolidated sediments must be taken at  
 280 sufficient depth to represent the crustal temperature gradient and not be perturbed by temperature variation in the  
 281 overlying water or ice (i.e. they must be representative of steady-state conditions). The penetration depth of  
 282 temperature variation is dependent on its frequency (Equation 4 and Fig. 4; Carslaw and Jaeger, 1959).  
 283 Consequently, diurnal or annual cycles only affect the upper few centimetres to couple of metres of the surface  
 284 temperature profile, whilst variations over the last 200-300 years will affect the upper 200 m, and post-glacial  
 285 warming can be observed down to 2500 m. These effects are dampened by an overlying water column or ice sheet,  
 286 but temperature variation over 10 kyr can still affect basal ice sheet temperatures (Engelhardt, 2004). Whilst large  
 287 ( $> 10^\circ\text{C}$ ) seasonal temperature variations are dampened by  $\sim 90\%$  at water depths of 3-5 m (Müller et al., 2016),  
 288 long-term variations (e.g. climate-controlled variations in Circumpolar Deep Water over the last  $\sim 12 \text{ kyr}$ ;  
 289 Hillenbrand et al., 2017) are likely recorded in the upper 3 m at 400 m water depth, 2 m at 700 m depth, and even  
 290 the upper  $\sim 1 \text{ m}$  at 1000 m depth (Dziadek et al., 2019).

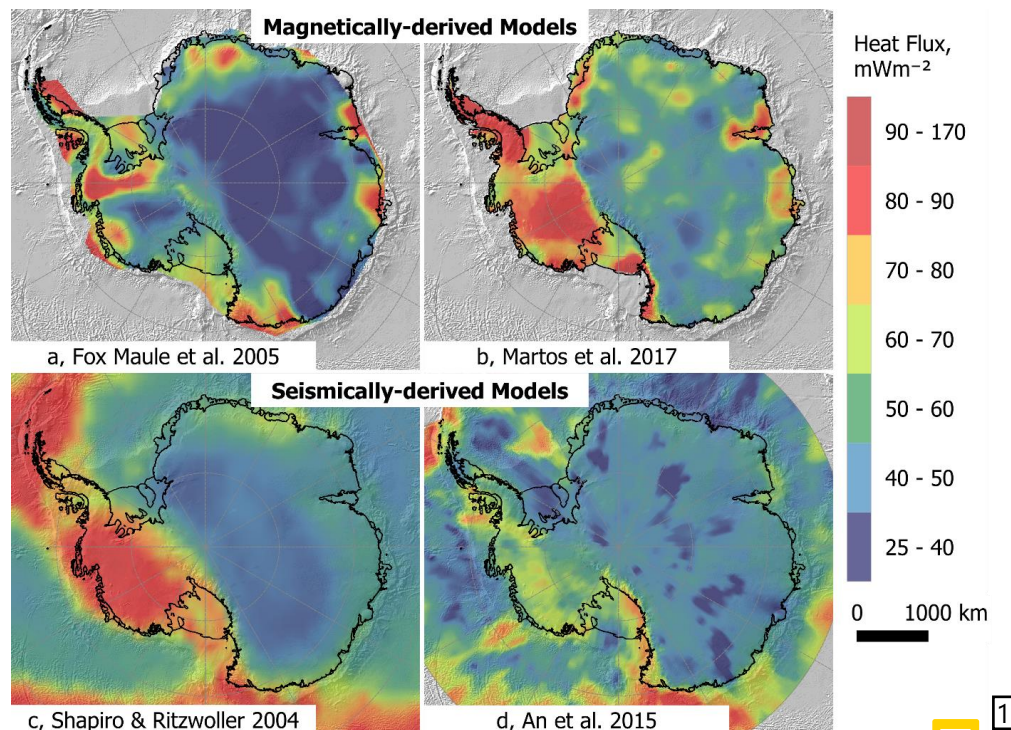
291 Similarly to borehole temperature measurements, a time delay must be considered between penetration of the  
 292 sediments and temperature measurement. A ten minute delay between sediment penetration and measurement is  
 293 sufficient to allow decay of frictional heating, as the temperature decay takes  $\sim 100 \text{ s}$  (Dziadek et al., 2019; Pfender  
 294 and Villinger, 2002).

This page contains no comments



295 **4. Geophysical and geological methods to estimate GHF**

296 In addition to the few and sparse penetrative GHF estimates in Antarctica, continental (Fig. 5) and regional (Fig.  
 297 6) estimates have been derived from both solid Earth (geophysical/geological), and glaciological data and models.



298  
 299 **Fig. 5. Continent-scale geophysical estimates of GHF derived from magnetic Curie depth estimates (a and b; Fox Maule**  
 300 **et al., 2005; Martos et al., 2017a) and seismic models (c and d; An et al., 2015a; Shapiro and Ritzwoller, 2004).**



Number: 1      Author: brice      Subject: Sticky Note      Date: 13/04/2020 11:27:21

---

A: Fox Maule et al., did you use the 2005 version of the data set or the updated one from Purucker ? Based on the figure, you are using the Purucker et al update so please cite:

M. Purucker. Geothermal heat flux data set based on low resolution observations collected by the champ satellite between 2000 and 2010, and produced from the mf-6 model following the technique described in fox maule et al.(2005). See <http://websrv.cs.umn.edu/isis/index.php>, 2013.

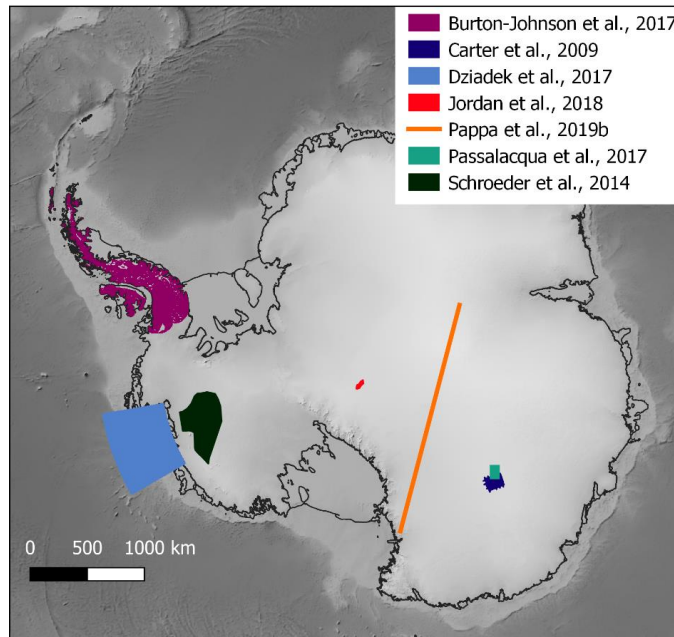


**Fig. 6. Coverage of sub-continental scale regional estimates of GHF.**<sup>1</sup>

#### 4.1. Magnetic methods deriving GHF from Curie depth.<sup>2</sup>

As for the penetrative methods of GHF estimation described above (Section 3), geophysical methods also derive GHF from a temperature gradient. In this case, magnetic survey data is used to determine the depth at which the maximum temperature of ferromagnetic magnetisation is exceeded (the Curie temperature; Haggerty, 1978). This Curie temperature is different for different minerals, but is assumed in these studies to the Curie temperature of magnetite (580 °C) as this mineral is most commonly the dominant contributor to crustal magnetisation (Bansal et al., 2011; Fox Maule et al., 2005; Langel and Hinze, 1998).

Above the Curie temperature, rocks lose their ability to maintain ferromagnetic magnetisation (e.g. Haggerty, 1978). The depth of this isotherm in the crust (the Curie Point Depth, CPD; Fig. 7 and Fig. 2) is thus assumed to be the depth to the bottom of the magnetic source (DBMS) determined from magnetic survey data. The DBMS maps a transition zone, rather than an exact depth (Haggerty, 1978), and can provide information on crustal temperatures at depths not accessible by other means (Andrés et al., 2018; Okubo et al., 1985). Regions found to have a shallower DBMS (and thus an assumed shallower CPD) are expected to have higher average temperature gradients, and, therefore, higher GHF (e.g. Aboud et al., 2011; Andrés et al., 2018; Arnaiz-Rodríguez and Orihuela, 2013; Bansal et al., 2013, 2011; Bhattacharyya and Leu, 1975; Guimarães et al., 2013; Li et al., 2017; Obande et al., 2014; Okubo et al., 1985; Ross et al., 2006; Salem et al., 2014; Tanaka et al., 1999; Trifonova et al., 2009).



Number: 1      Author: brice      Subject: Inserted Text      Date: 13/04/2020 11:27:49

---

I would suggest to be very explicit about what each data set is in that figure. e.g. Passalacqua et al., 2017: "radar reflectivity and inverse modelling". Provide a table with the links to the data sets ?  
(see general comments)



Number: 2      Author: brice      Subject: Inserted Text      Date: 10/04/2020 15:51:30

---

derived estimates (to be consistent with the other sub-section title )



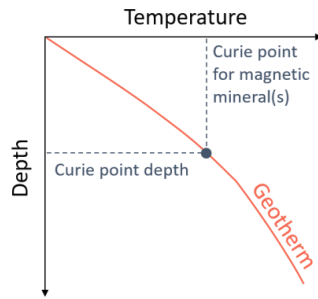


**Fig. 7. Approximation of the geothermal gradient from the Curie point depth (CPD). The Curie point depth is assumed to mark the base of the magnetic crust (DBMS).**

The first Antarctic-wide magnetically-derived GHF map (Fox Maule et al., 2005; Fig. 5a) used the “equivalent source magnetic dipole method” (Mayhew, 1979) to map magnetic anomalies from multiple satellites at different altitudes as evenly distributed magnetic dipoles on the Earth’s surface (Dyment and Arkani-Hamed, 1998). Due to filtering of the data during processing, this magnetic anomaly distribution is only susceptible to shallow, short-wavelength magnetic variation. To calculate the CPD, a long-wavelength CPD model was modified until it reproduced the determined short-wavelength anomalies. The temperature gradient represented by this CPD was combined with assumed homogenous crustal properties (heat production and conductivity) to model the surface heat flow. Due to the high altitude of the satellite data, the horizontal resolution of this approach was limited to at least a few hundred kilometres.

Spectral methods are the alternative and more commonly applied approach to estimating the DBMS, analysing the spectrum of wavelengths in magnetic profiles or gridded data (e.g. Blakely, 1996; Okubo et al., 1985; Spector and Grant, 1970). These methods depend on the implicit assumption that long wavelength features result from deep sources. The depth of this source is calculated from a “power spectrum” (Fig. 8) of wavenumber (the inverse of the wavelength) against the logarithm of each wavenumber’s “power” (the square of each wavelength’s magnitude after conversion by a Fast Fourier Transformation to describe the spectrum of wavelengths in the signal). From this power spectrum (Fig. 8) the top ( $Z_t$ ) and centre ( $Z_0$ ) of the deepest magnetic layer are inferred from the slope of the intermediate and long wavelength zone of the spectra derived from magnetic anomaly data. The DBMS ( $Z_{DBMS}$ ) stems from the simple geometric relationship between these depths:

$$Z_{DBMS} = 2Z_0 - Z_t$$

(6)



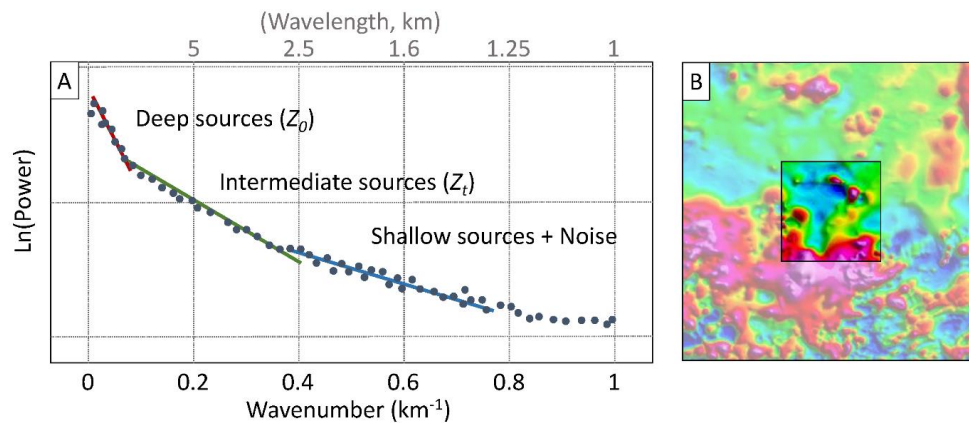


**Fig. 8. A) Identification of the slopes of the intermediate and long wavelength magnetic anomalies from the power spectrum of magnetic anomalies within a single magnetic window (B).** Illustration, small circular anomalies in the magnetic window would correspond to shallow sources in the power spectrum, whilst larger anomalies would correspond to intermediate and deep sources.

To map the DBMS across a study area, the spectra of magnetic anomalies are computed within overlapping rectangular windows regularly spaced over the aeromagnetic map. Particularly for gridded data, the dimensions of the region chosen to analyse the long wavelength frequencies must be sufficiently large to capture the DBMS. Ravat et al. (2007) elaborate that the dimension of the region analysed may need to be (in some cases) up to 10 times the DBMS, but that dimensions exceeding 200 to 300 km may average different large-scale crustal structures. This suggests that satellite data, which typically detects magnetic anomalies in that wavelength, may not be suitable for this spectral method of CPD estimation. Choosing the window size therefore forces a trade-off between accurately determining the DBMS within each sub-region and resolving small changes in DBMS between sub-regions (Ross et al., 2006).

Spectral methods have been applied in Antarctica (Dziadek et al., 2017; Martos et al., 2017a; Purucker and Whaler, 2007; Fig. 5b and Fig. 6) to combined satellite and airborne magnetic anomaly data (e.g. ADMAP; Golynsky et al., 2006; Maus, 2010). The results show a general agreement at a continental scale, but vary significantly on a regional scale (Fig. 5). This is related to the resolution of the magnetic anomaly data, particularly in regions where only satellite magnetic data are available. Furthermore, regional-scale magnetic anomaly databases are usually a mosaic of individual aeromagnetic surveys. Ross et al. (2006) emphasise that subtle discontinuities along survey boundaries are caused by differences in survey specifications, such as flight line spacing, flight altitude, regional field removal, or the quality of data acquisition. These, for instance, may contaminate the long-wavelength signal caused by deep magnetic sources (Grauch, 1993). Long wavelength features can also result from shallow but spatially extensive sources, such as volcanic provinces, and can lead to an underestimation of the DBMS.

CPD estimates assume a homogenous magnetic mineralogy of magnetite, and thus a Curie temperature of 580 °C (Bansal et al., 2011; Fox Maule et al., 2005; Langel and Hinze, 1998). This assumption neglects the compositional variability in plutonic rocks that lead to Curie temperature ranges between 300 °C and 680 °C, and in cases of



---

Number: 1      Author: brice      Subject: Inserted Text      Date: 10/04/2020 11:58:14

---

. B)



---

Number: 2      Author: brice      Subject: Cross-Out      Date: 10/04/2020 11:59:10

---



---

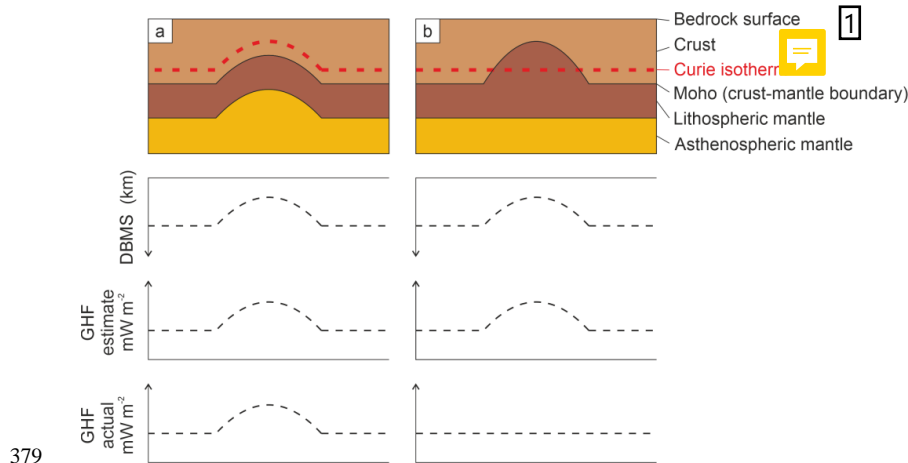
Number: 3      Author: brice      Subject: Inserted Text      Date: 10/04/2020 11:59:26

---

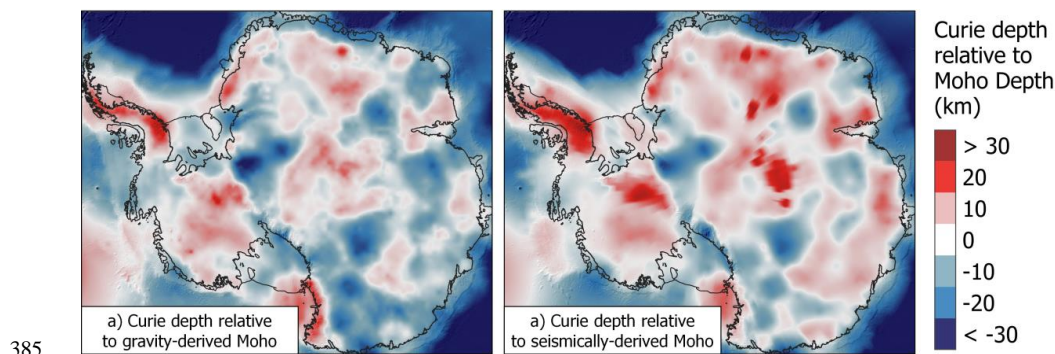
highlighted



371 magnetic assemblages of Fe-Ni-Co-Cu metal alloys up to 620 °C to 1084 °C (Haggerty, 1978). Without further  
 372 constraints and validations, these assumptions remain the best approach, especially in sparsely sampled regions  
 373 like Antarctica, but introduce uncertainties of several kilometres in Curie depths and consequent uncertainties in  
 374 GHF estimates (Bansal et al., 2011; Ravat et al., 2007). Similarly, in areas of thin crust, non-magnetic mantle  
 375 rocks can be shallower than the Curie depth. In these regions, the calculated Curie isotherm will appear shallower  
 376 due to a lack of magnetic minerals in the mantle rocks (Fig. 9.; Frost and Shive, 1986; Wasilewski and Mayhew,  
 377 1992). This can be investigated through comparison of the Antarctic Curie depth estimates with the seismically-  
 378 or gravitationally-derived depth of the crust-mantle boundary (the Moho depth; Fig. 10 and Fig. 2).








380 **Fig. 9.** Two scenarios illustrating the ambiguity in estimating Curie isotherm depth and GHF. a) Estimates from a  
 381 region with a shallow Curie isotherm over an area of thin crust. b) Similar but incorrectly interpreted estimates from  
 382 a region of shallow non-magnetic mantle rocks. In scenario (b), the DBMS is shallower despite there being no deviation  
 383 in the Curie isotherm depth. DBMS [3] pth to the Bottom of the Magnetic Source [4] assumed to represent the Curie  
 384 depth in the GHF estimates discussed).



386 **Fig. 10.** Comparison of Curie depth (Martos et al., 2017) and depth of the crust-mantle boundary (the Moho depth)  
 387 derived from a) gravity modelling (Pappa et al., 2019b), and b) seismic modelling (An et al., 2015a). Negative values  
 388 show areas where the estimated Curie depth is deeper than [5] the estimated Moho depth, and positive values are where  
 389 the Curie depth is shallower than the Moho depth.

## Page: 15

- 
-  Number: 1    Author: brice    Subject: Sticky Note    Date: 10/04/2020 12:02:28  
CPD
- 
-  Number: 2    Author: brice    Subject: Cross-Out    Date: 10/04/2020 12:05:04
- 
-  Number: 3    Author: brice    Subject: Inserted Text    Date: 10/04/2020 12:05:06  
.
- 
-  Number: 4    Author: brice    Subject: Inserted Text    Date: 10/04/2020 12:05:00  
bottom of the magnetic source
- 
-  Number: 5    Author: brice    Subject: Sticky Note    Date: 13/04/2020 11:29:37  
As is, to me, this figure illustrates more the difference between Martos et al. (2017) and the two methods than between seismic and gravity modeling. Why not simply plot the difference between the two methods you describe?



390 However, whilst in general the Earth's mantle does not contribute to the magnetic signal (due to its weak  
391 magnetisation and high temperature conditions), in some cases the Curie depth may indeed lie within the mantle.  
392 This occurs where metallic magnetic phases in the mantle beneath old, tectonically stable crust ("cratons"; Ferré  
393 et al., 2013) or subduction regions (e.g. Blakely et al., 2005) contribute to mantle magnetisation. In these settings  
394 the crust-mantle boundary should not be considered an absolute magnetic boundary (Ferré et al., 2013). This  
395 implies that if in a given region the Moho depths are shallower than the deepest magnetic layer, a magnetic mantle  
396 at temperatures below the Curie temperature may be considered. However, even in these cases the upper mantle  
397 susceptibility will be more than 1-2 magnitudes smaller than the overlying crust. This is not considered in current  
398 spectral methods assuming constant susceptibility. Consequently, Curie depth methods yield non-unique  
399 solutions, and further available constraints and observations need to be considered, when interpreting the Curie  
400 temperature distribution (e.g. geological evidence, borehole measurements, and Moho depth estimates).

#### 401 4.2. Seismic estimates<sup>1</sup>

402 Temperature is the dominant control on seismic velocity in the mantle (e.g. Carlson et al., 2005), and hence the  
403 mantle heat flow at the base of the Antarctic crust can be determined from seismic data. By determining the change  
404 in seismic velocities marking the density discontinuity at the lithosphere-asthenosphere boundary (Fig. 2) the  
405 depth of the 1330°C isotherm can be estimated. This is the "mantle adiabat" marking the top of the seismic low-  
406 velocity zone, and the change from a solid to ductile mantle (Fig. 2). The continental-scale GHF can then be  
407 estimated by assuming the heat production and conductivity of the lithosphere above this boundary, and  
408 integrating this with the seismically-derived mantle heat flow (An et al., 2015b; Fig. 5d). However, the  
409 seismically-derived, continent-scale Antarctic GHF model of An et al. (2015a) (Fig. 5d) is limited to a lateral  
410 spatial resolution of >120 km, assumes a laterally uniform crustal structure, and is insensitive to the lithospheric  
411 geotherm (instead it inversely correlates with crustal thickness).

412 Composition also affects seismic velocities. For example, a 2% increase in velocity can be explained either by a  
413 120°C decrease in temperature, a 7.5% depletion in iron, or a 15% depletion in aluminium (Godey et al., 2004).  
414 Slow mantle velocities at subduction zones can also be caused by water or hydrous fluids serpentinising the mantle  
415 wedge (Fig. 2; Kawakatsu and Watada, 2007). However, velocity in the Antarctic seismic model (An et al., 2015b)  
416 does not account for variability of mantle compositions, mineralogy, grain size, or water content of the mantle or  
417 crust. An uncertainty in the lithospheric thickness of 15-30 km was assumed by (An et al., 2015b) based on the  
418 150°C temperature uncertainty, but ~50 km uncertainty for ~200 km thick lithosphere may be more accurate  
419 (Artemieva, 2011; Godey et al., 2004). In addition, seismological models suffer from limited and inconsistent  
420 spatial coverage, which can lead to discrepancies in upper mantle velocities and differences in Moho depths (Fig.  
421 2) up to 10 km, even for the same receiving station (An et al., 2015b supporting information; Pappa et al., 2019).

422 Some constraints on the mantle and lithosphere composition can be determined from xenoliths (rock fragments  
423 of the deep crust or mantle entrained in magma rising from depth) or exposed deep crustal sections, where  
424 variation in temperature and composition with depth can be determined from the metamorphic minerals present.  
425 Constraints can also be derived empirically by comparing the seismic velocity with similar regions. Shapiro and  
426 Ritzwoller (2004) (Fig. 5c) extrapolated global heat flow measurements to Antarctica based on the assumption  
427 that structurally similar regions have similar magnitudes of GHF. This was achieved by calculating a spatially



derived estimates (see 4.1)





variable “similarity functional” determined from the differences between the seismic velocity and seismic Moho depth between a location of interest and a comparable location elsewhere. A histogram of heat flow measurements could then be assigned to the location of interest in Antarctica based on the similarity-weighted sum of measurements from structurally similar regions, and the mean values of these distributions mapped as continental heat flow. Spatial resolution was limited to the lateral resolution of the global shear velocity model across Antarctica (600-1000 km; Shapiro and Ritzwoller, 2002). Although the studies of Shapiro and Ritzwoller (2004) and An et al. (2015a) both used seismic data and are thus frequently compared, it is important to highlight that they use very different approaches in deriving heat flow (the former employing a probabilistic approach and the latter using forward modelling).<sup>[1]</sup>


#### 4.3. Gravity modelling<sup>[2]</sup>

Satellite gravity data has been used as an alternative to seismic modelling to determine crustal thickness. Pappa et al. (2019b) used satellite gravity data, a model of global gravity variation (the “geoid”), surface and bedrock topography, and assumed rock and ice densities to calculate the topographically-corrected variation of gravity in Antarctica (the “Bouguer anomaly”), from which the depth of the crust-mantle boundary could be calculated. This approach to calculate crustal thickness is sensitive to long-wavelength (>150 km) features representing deep structures, rather than short-wavelength, near surface density changes. However, gravity-modelling solutions are non-unique, and require additional constraints on the density contrast between the crust and mantle at a reference depth, and/or seismic depth constraints on crustal thickness.

Using the gravity-derived crustal thickness estimates, cross-sectional models of the mantle and lithospheric structure were calculated, with adjustments made to crustal density and crustal thickness until the models reflected the observed variation in gravity and elevation (Pappa et al., 2019b). By assigning assumed values of heat productivity and thermal conductivity values to the modelled cross-sections, surface heat flow was calculated along the line of the modelled cross-section (Fig. 6). A 3D lithospheric model has since been published (Pappa et al., 2019a), and a map of Antarctica’s resultant estimated GHF is in preparation for publication (pers. comms.).


#### 4.4. Conjugate margins<sup>[3]</sup>

An alternative approach to constrain the probable GHF of East Antarctica is to compare it with its Gondwanan conjugate margins, reconstructed prior to the breakup of the supercontinent (Fig. 11). Plate tectonic reconstructions indicate that the subglacial geology of East Antarctica is comparable to the margins of Australia, Africa, and India (Aitken et al., 2016; Daczko et al., 2018; Ferraccioli et al., 2011; Flowerdew et al., 2013; Mulder et al., 2019). By kriging the heat flow measurements of the continents in their pre-Gondwana breakup arrangement, Pollett et al. (2019) interpolated a heat flow surface through Antarctica and its conjugate margins (Fig. 11). This method highlighted similarities and differences between the most recent seismic and magnetically derived geophysical models of Antarctic heat flow (An et al., 2015b; Martos et al., 2017) with the better constrained heat flow of the conjugate margins. In particular, this approach showed reasonable agreement along the margin with Africa, but an absence in either the magnetic or seismic models of high heat flow provinces in East Antarctica comparable with south Australia; an absence of the low heat flow of SW Australia in the magnetically derived model of East Antarctica (Martos et al., 2017); and an absence of the high heat flow of

 Number: 1      Author: brice      Subject: Inserted Text      Date: 13/04/2020 11:29:47


---

Thanks for pointing this difference out !

 Number: 2      Author: brice      Subject: Inserted Text      Date: 10/04/2020 15:53:14

---

model derived estimates (e.g)

 Number: 3      Author: brice      Subject: Inserted Text      Date: 10/04/2020 15:53:52

---

as before for the sub-title.



northern India in the seismically derived model of East Antarctica (An et al., 2015b). However, when extrapolating heat flow away from the conjugate margins into the interior of Antarctica, this approach is susceptible to the method of interpolation used and the quality and scarcity of the borehole-derived GHF estimates in the interior of Antarctica (Section 3).

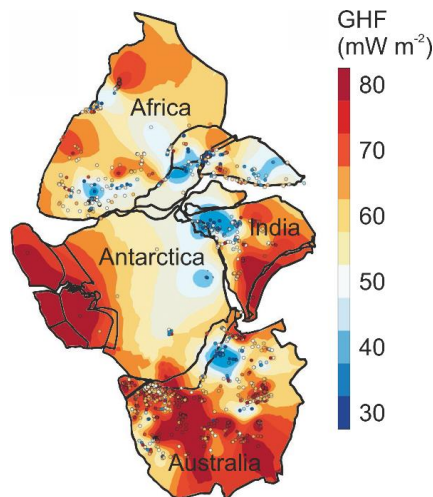


**Fig. 11.** Interpolated heat flow map of Gondwana, showing the derivation of Antarctic GHF from the reconstructed conjugate margins of the supercontinent. Terrestrial heat flow data shown by points. Adapted from Pollett et al. (2019).

#### 4.5. Isostatic elevation

In addition to crustal thickness and density, the thermal state of the lithosphere also contributes to its isostasy and observed surface elevation. The effect of thermal isostasy on the bathymetry of oceanic crust is well recognised: as oceanic crust migrates from the spreading ridge it cools, thickens, contracts, and subsides (Stein and Stein, 1992). However, the effect of thermal isostasy on continents is masked by compositional contributions to isostatic elevation (i.e. lateral variations in crustal thickness and density, Fig. 12a; Hasterok and Chapman, 2007b, 2007a).

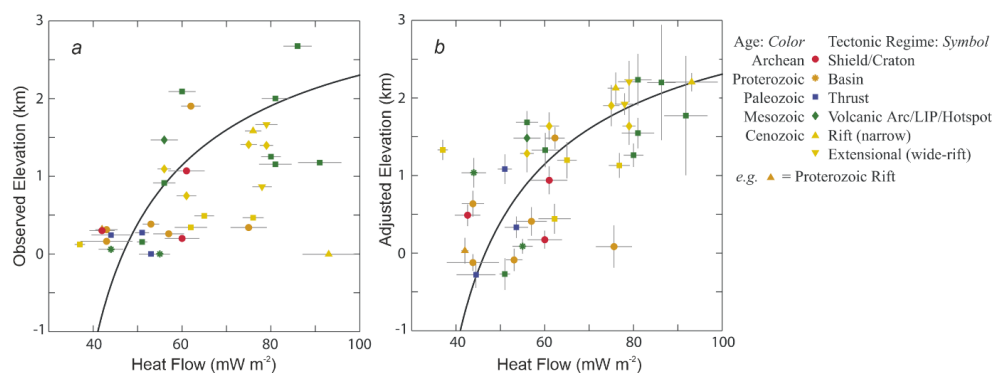


**Fig. 12.** Relationship of the median observed (a) and adjusted (b) elevation and median compiled heat flow values of 36 geological provinces on the land and continental shelves of North America, ranging from 30 - 2082 x 10<sup>3</sup> km<sup>2</sup>. Compiled



---

Number: 1      Author: brice      Subject: Inserted Text      Date: 10/04/2020 15:55:09

---

Can you provide some numbers on the maximum and minimum GHF ?



---

Number: 2      Author: brice      Subject: Sticky Note      Date: 13/04/2020 11:20:21

---

Section 4.5 is quite long compared to the other subsections, and describes in a lot of detail a technique that is not widely used in Antarctica because of the lack of measurements. It seems therefore that including specific equations is superfluous, and perhaps the paragraph on its application in Antarctica could then be extended.



481 heat flow data excluded values outside of the range 20 - 120 mW m<sup>-2</sup> as these values were most likely affected by near  
 482 surface processes (e.g. hydrothermal circulation) or shallow magmatism, and do not reflect the lithosphere's thermal  
 483 state. Observed elevations are converted to adjusted elevation by normalising according to their seismically-derived  
 484 crustal thickness and crustal density and an equation for thickness and density-based isostasy. The black curve shows  
 485 the best-fitting thermal-isostatic model for North American adjusted elevation and heat flow. Adapted from Hasterok  
 486 and Chapman (2007a).

487 Hasterok and Chapman (2007b, 2007a) developed a methodology for investigating thermal isostasy in the  
 488 continental lithosphere by normalising the observed elevation using an isostatic correction. The normalised  
 489 elevation ( $\varepsilon'$ ) is calculated from Equation 7 (Han and Chapman, 1995):

$$\varepsilon' = \varepsilon + h'_c \left( 1 - \frac{\rho'_c}{\rho_m} \right) - h_c \left( 1 - \frac{\rho_c}{\rho_m} \right)$$

491 (7)

492 Where  $\varepsilon$  is the observed elevation;  $h_c$  and  $\rho_c$  are respectively the seismically-derived crustal thickness and density  
 493 of the study area;  $h'_c$  and  $\rho'_c$  are the thickness and density respectively of a standard crustal column; and  $\rho_m$  is  
 494 the mantle density. When the crust is below sea level, an additional term including bathymetric water depth ( $\varepsilon_{obs}$ )  
 495 and seawater density ( $\rho_w$ ) are included (Equation 8; Han and Chapman, 1995):

$$\varepsilon' = \varepsilon + h'_c \left( 1 - \frac{\rho'_c}{\rho_m} \right) - h_c \left( 1 - \frac{\rho_c}{\rho_m} \right) - \left( \frac{\varepsilon_{obs} \rho_w}{\rho_m} \right)$$

497 (8)

498 Compositionally corrected elevation generally increases with increasing surface heat flow (Fig. 12b). By  
 499 differentiating the different contributions to isostatic elevation, it was shown that crustal thickness and density  
 500 contribute ~3 km of the observed elevation range of North America, and thermal isostasy contributes a further ~3  
 501 km; similar in magnitude to the effect of thermal isostasy on oceanic lithosphere (Hasterok and Chapman, 2007a,  
 502 2007b). However, there are uncertainties in the thermal isostasy model associated with the assumed properties,  
 503 including thermal conductivity, thermal expansion, and heat production in the upper and lower crust, of which  
 504 uncertainty in upper crustal heat production has the largest effect (Hasterok and Chapman, 2007b). Uncertainties  
 505 in the seismic data used for calculating crustal thickness and density affect the uncertainty of the compositional  
 506 isostatic correction (Equations 7 and 8; Hasterok and Chapman, 2007b).

507 This approach was used to derive the thermal contribution to isostatic elevation of Australia and North America,  
 508 and estimate the continental sub-lithospheric and radiogenic heat flow (Hasterok and Chapman, 2007b; Hasterok  
 509 and Gard, 2016). Whilst in general, the compositionally corrected elevation and surface heat flow values followed  
 510 the modelled curve for thermal isostatic equilibrium (Fig. 12b), anomalous regions lie away from this curve. These  
 511 anomalies result from: 1) additional sources of buoyancy and/or dynamic support (e.g. anomalously buoyant  
 512 mantle lithosphere); 2) anomalous surface heat flow, not representative of the deeper thermal regime (e.g. high  
 513 concentration of heat producing elements in the shallow crust); 3) deviations from the thermal properties of the  
 514 reference crustal model (e.g. heat production); or 4) combinations of these properties (Hasterok and Gard, 2016).

This page contains no comments



Although developed for regions of known heat flow, application of this approach to Antarctica (Hasterok et al., 2019) may provide an alternative estimate of heat flow based largely on two well-constrained variables: surface and bedrock topography. However, it is dependent on the quality of seismic constraints on crustal thickness and density as well as constraints on the heat production and thermophysical properties of the upper crust. For example, regions where high surface heat flow is dominantly from anomalously high upper crustal heat production will have lower elevations than regions of similar surface heat flow but with lower upper crustal heat production. Crust that has experienced tectonic and magmatic activity in the Cenozoic (i.e. <66 Ma) may be in a transient rather steady-state thermal regime, so this approach may have challenges in West Antarctica. Steady-state thermal modelling is thus more applicable to the old, stable crust of East Antarctica; particularly if the heat flow and isostasy of the conjugate margins are considered (Hasterok and Gard, 2016; Pollett et al., 2019). However, differences between the crustal thickness based on gravity modelling and isostatic elevation modelling may indicate variable densities and/or compositions of the underlying mantle (Pappa et al., 2019b, 2019a).

#### 4.6. Enhancement of GHF estimates by incorporation of heterogeneous crustal compositions

The geophysical approaches described above assume laterally homogenous heat production in the crust. However, given the geologically heterogeneous composition of the crust, it is important to consider the effects of variable lithospheric heat production and incorporate this into forward models of GHF.

Radiogenic heat production in the upper crust contributes an estimated 26-40 % of the total continental GHF (Artemieva and Mooney, 2001; Hasterok and Chapman, 2007b, 2011; Pollack and Chapman, 1977; Vitorello and Pollack, 1980). Radioactive isotopes of the heat producing elements (HPEs) uranium, thorium, and potassium (U, Th, and K) are responsible for ~98% of lithospheric heat production (Beardsmore and Cull, 2001). These elements are incompatible with mineral structures in the mantle and lower crust, so concentrate in the upper crust and decrease in abundance with depth during planetary differentiation (the chemical and physical separation of an initially homogenous planetary body into one with an iron-rich core, magnesium-silicate-rich mantle, and a thin silicate-rich crust; Roy et al., 1968; Rudnick and Fountain, 1995).

The upper crust itself is highly heterogeneous in composition. HPE distribution is determined by their compatibility in different minerals, concentrating them in Si-rich silicic rocks (e.g. granite or rhyolite) relative to Fe-rich mafic rocks (e.g. gabbro or basalt). Immature sediments inherit the HPE abundance of their eroded source rocks, but decrease in HPE abundance with increasing maturity and the consequent decrease in their lithic contents (Burton-Johnson et al., 2017; Rybach, 1986). Crustal heat production is thus heterogeneous, and the most significant control of HPE abundance and resultant heat production in the lithosphere is the distribution of the composite lithologies of the upper crust (Lachenbruch, 1968; Sandiford and McLaren, 2002; Taylor and McLennan, 1985).

##### 4.6.1. Whole rock geochemical analysis of heat production

Heat production of exposed lithologies can be determined from their concentrations of HPE (U, Th, and K) determined by geochemical analysis, or by airborne or ground-based gamma ray surveys. Radiogenic heat production for each sample ( $H$ ,  $\mu\text{Wm}^{-3}$ ) for the present day ( $t=0$ ) can be determined from Equation 9 (Turcotte and Schubert, 2014):

This page contains no comments





$$H = (0.9928C_0^U H^{U238} + 0.0071C_0^U H^{U235} + C_0^{Th} H^{Th232} + 0.000119C_0^K H^{K40})D$$

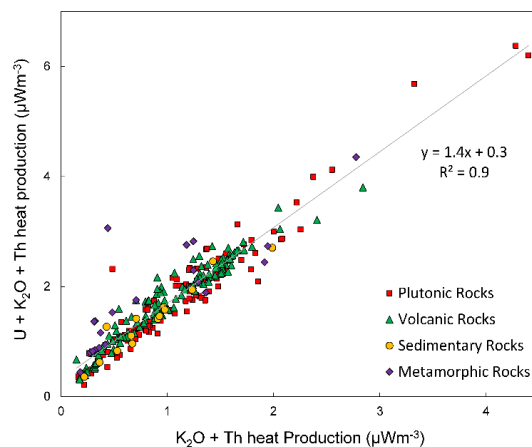
(9)

Where  $C_0^U$ ,  $C_0^{Th}$  and  $C_0^K$  are the measured concentrations (ppm) of U, Th and K respectively;  $H^{U238}$ ,  $H^{U235}$ ,  $H^{Th232}$  and  $H^{K40}$  are the heat productivities of the respective isotopes  $^{238}\text{U}$  ( $9.37 \times 10^{-5} \text{ Wkg}^{-1}$ ),  $^{235}\text{U}$  ( $5.69 \times 10^{-4} \text{ Wkg}^{-1}$ ),  $^{232}\text{Th}$  ( $2.69 \times 10^{-5} \text{ Wkg}^{-1}$ ) and  $^{40}\text{K}$  ( $2.79 \times 10^{-5} \text{ Wkg}^{-1}$ ); and  $D$  is the assumed density of the rock (e.g. 2800, 2850, and  $3000 \text{ kg m}^{-3}$  for felsic, intermediate, and mafic granulites, respectively; Hasterok and Chapman, 2011). When using geochemical data to calculate heat production, this allows new and archive data to be used to calculate the heat production of the sampled outcrop. However, many archive analyses occurred prior to the development of accurately U quantification (e.g. by high resolution XRF or ICP-MS). An empirical relationship (Equation 10; Burton-Johnson et al., 2017) allows calculation of total U, Th, and K heat production ( $H$ ) from samples possessing only Th and K data ( $H_{K,Th}$ ; correlation coefficient,  $R^2 = 0.9$ ; Fig. 13).

$$H = 1.4H_{K,Th} + 0.3$$

(10)

Heat production values can be assigned to bedrock geology either by interpolation of the point values or by assigning the point values to the mapped geology and assigning their average value to the geological unit; the average being either the mean (Veikkolainen and Kukkonen, 2019), area weighted mean (Slagstad, 2008), or median value (Burton-Johnson et al., 2017). Interpolation shows spatial variability within a unit, but is affected by the interpolation method used, requires sufficient and evenly distributed data coverage, and is affected by anomalous values. For these reasons, the median values were used for the unevenly distributed archive data of the Antarctic Peninsula (Burton-Johnson et al., 2017). In Antarctica, this approach has been applied to the Antarctic Peninsula (Burton-Johnson et al., 2017; Fig. 6) and along coastal outcrops in East Antarctica (Carson et al., 2014; Carson and Pittard, 2012). These studies integrated their maps of variable lithospheric heat production with geophysical models of the deeper heat flow to estimate the total GHF at the bedrock surface.



575



Simplify in one sentence.



Fig. 13. The relationship between total calculated heat production from U, K<sub>2</sub>O and Th decay and the heat production values from K<sub>2</sub>O and Th only for different broad lithologies, enabling total heat production calculation from incomplete archive data (n = 319; Burton-Johnson et al., 2017).

#### 4.6.2. Gamma ray spectrometry

Rather than whole rock geochemical analysis, the gamma ray spectrum can be used to determine the concentrations of radioactive isotopes, including those of K, Th, and U, and was first used for U exploration. Gamma ray spectrometry can be surveyed in the field, on samples, or from the air. Airborne surveys can cover large areas, and have been used to survey Western Australia, SW England, and all of Finland (Beamish and Busby, 2016; Bodorkos et al., 2004; Hyvönen et al., 1972). However, the data requires multiple corrections, and the recorded data integrates the radiation from the bedrock, surface cover (including soil and vegetation), the atmosphere, cosmic radiation, and the aircraft, making the data less accurate than ground measurements or sample analysis (Veikkolainen and Kukkonen, 2019). The technique is only sensitive to the upper 25cm of the land surface, with overlying sediments and water bodies masking the radiation and leading to underestimates of heat production (Phaneuf and Mareschal, 2014). However, if the signal could be linked to mapped geological units and other evidence for subglacial geology (e.g. aeromagnetic and gravity anomalies) it may be feasible to extrapolate the calculated heat production beneath the ice sheet. Hand-held gamma ray spectrometry studies, where heat production can be correlated with lithology along exhumed crustal profiles, show promise in this regard elsewhere (Alessio et al., 2018).

#### 4.6.3. Crustal structure

Whilst surface HPE distribution can be constrained by measurements, the vertical distribution is more ambiguous. In heat flow models, heat production is often assumed to decrease exponentially with depth (e.g. Fox Maule et al., 2005; Martos et al., 2017). This exponential model was developed to explain observations from exposures of large, thick composite granite bodies (batholiths) where magma was initially emplaced at different depths in the crust (Lachenbruch, 1968, 1970; Swanberg, 1972) and reflects a proposed decrease in HPE abundance with increasing metamorphic grade (Lachenbruch, 1968; Sandiford and McLaren, 2002). However, this relationship has been challenged by other studies comparing HPE abundance and metamorphic grade (Alessio et al., 2018; Veikkolainen and Kukkonen, 2019), showing that the lithological change from the largely silicic upper crust to the mafic lower crust has a larger influence on HPE abundance than metamorphic grade (Bea, 2012; Bea and Montero, 1999). Deep (9–12 km) boreholes also show a correlation of heat production with lithology, but not with depth (Clauser et al., 1997; Popov et al., 1999). In fact, heat production *increased* for the first 2 km of the 12 km superdeep well of the Kola Peninsula, Russia, then remained variable but high with increasing depth (Popov et al., 1999). Similarly, heat production increases below 3 km in the recent 5 km UD-1 well of the Cornubian Batholith, UK (Dalby et al., 2020). As such, the available evidence indicates that the first-order HPE distribution is controlled by the HPE abundance of the crust prior to metamorphism and the vertical distribution of the crust's composite rock types. Inversely, it indicates that HPE distribution is not controlled by depth in the crust or the degree of metamorphism resulting from the increase in pressure and temperature.

Without evidence for the deeper structure of the crustal column, the lithological and HPE distribution of the lithosphere can instead be modelled as layers of variable thickness and heat production: the upper crust, middle

This page contains no comments



crust, lower crust, and mantle lithosphere. Surface heat flow is largely insensitive to variations in the heat production or thickness of the mafic lower crust and mantle lithosphere due to their heat production being ~1-2 orders of magnitude lower than that of the upper crust (Hasterok and Chapman, 2011; Rudnick and Fountain, 1995; Rudnick et al., 1998). The middle crustal layer can either be excluded (Hasterok and Chapman, 2011) or treated as a layer of invariable heat production (e.g. An et al., 2015, for Antarctica) due to its low heat production compared with the range of the upper crust. Lithospheric heat production can thus be defined by the heat production and relative thickness of the upper crust, or upper crustal heat producing layer (Hasterok and Chapman, 2011). This can be defined by:

$$Q_s = Q_b + H_{UC}D = FQ_s + H_{UC}D = H_{UC}D/(1 - F)$$

(11)

Where  $Q_s$  is the surface heat flow,  $Q_b$  is the basal heat flow of the upper crust,  $H_{UC}$  is upper crustal heat production,  $D$  is the thickness of the upper crustal heat producing layer, and  $F$  is the proportion of the surface heat flow contributed by the basal heat flow ( $Q_b$ ) (adapted from Hasterok and Chapman, 2011).

Rather than a simple layered model, more complex 2D or 3D models of upper crustal structure can be developed using geophysical data, and the 2D or 3D crustal units assigned heat production and conductivity values based on analyses of representative exposures. A 3D crustal model derived from gravity and aeromagnetic data was developed to map heat flow in Norway (Ebbing et al., 2006; Olesen et al., 2007). In Antarctica, this has been applied in 2D to the high heat production granites of the Ellsworth-Whitmore Mountains using airborne magnetic and gravity data and bedrock topography (Leat et al., 2018), and the Transantarctic Mountains using topography and satellite gravity data (Pappa et al., 2019b).


Whilst variability in deep lithospheric heat production has a smaller effect on surface heat flow than variability in upper crustal heat production (Hasterok and Chapman, 2011), it is not homogenous. These thermophysical properties can be constrained from deep xenoliths (fragments of rock entrained in magma rising from depth) (Hasterok and Chapman, 2011; Martin et al., 2014) and crustal sections (Berg et al., 1989), which can also inform on the local geothermal gradient at the time of their crystallisation.

To help constrain the properties of the Antarctic mantle, including its influence on Antarctic heat flow, a Geological Society of London Memoir is currently being compiled summarising the data gained from mantle xenoliths (Martin and van der Wal, in prep.). This includes a sample database, and a compilation of their grain size and water content. These xenoliths are from shallow sources, as their occurrence is biased towards areas of crustal rifting where the lithosphere is thinner, although some xenoliths are from deeper sources (e.g. from the Amery Rift and Ferrar Dolerite).

#### 4.6.4. Detrital material


Whilst heat production can be determined for exposed bedrock, the likely heat production of the rocks beneath the Antarctic ice sheet is harder to constrain. To investigate East Antarctica, glacial clasts were sampled from moraines adjacent to the Transantarctic Mountains (Goodge, 2018). Granitic samples older than 500 Ma (Ross Orogen) were selected as likely lithologies of the interior of East Antarctica, as these are the dominant lithologies

---


 Number: 1      Author: brice      Subject: Underline      Date: 10/04/2020 16:14:16

You use whilst several times, you could remove some of them.

---

 Number: 2      Author: brice      Subject: Underline      Date: 10/04/2020 16:15:18

---

 Number: 3      Author: brice      Subject: Inserted Text      Date: 10/04/2020 16:18:25

you can also cite: J. W. Goodge, C. M. Fanning, C. M. Fisher, and J. D. Vervoort. Proterozoic crustal evolution of central East Antarctica: Age and isotopic evidence from glacial igneous clasts, and links with australia and laurentia. Precambrian Research, 299:151–176, 2017.



of other Precambrian cratons (>542 Ma regions of tectonically-stable continental crust; e.g. central Canada). These clasts were analysed for their HPE abundance and attributed to their likely source area (the drainage basin of their associated glaciers). A probable range of subglacial heat flow values was estimated by assuming mantle and lower crustal GHF values and a thickness for the upper crust based on other Precambrian shields. This indicates that East Antarctic heat flow is comparable to other Precambrian cratons, and comparable to geophysical models of East Antarctic heat flow (Jeffering and Pattyn, 2013). However, broader application of this approach is biased towards more erosion resistant rock types, whilst less competent lithologies will not be preserved after glacial transport and deposition.

## 5. Glaciological inverse estimation of GHF

Although geothermal heat flow has a geological derivation, it can also be constrained by multiple approaches through its observable effects on the overlying ice sheet. Rather than using a forward modelling approach (i.e. determining the geological contributions and estimating their resultant heat flow), an inverse modelling approach can be applied by modelling observed glaciological properties (e.g. glacial flow and melt rates) and calculating the required heat flow. We will describe in this section different methods used in glaciology to derive GHF.

### 5.1. Subglacial water

The presence of subglacial water can be detected with a ground penetrating radar. The reflective properties of the ice-bedrock interface depend on the presence of water and, with certain caveats, radar surveys can be used to map subglacial water. In general terms, a glaciological model can then be used to estimate the values of GHF that better predict where basal temperatures reach the pressure melting point and melting occurs. We will describe in this Section examples of this approach.

Carter et al. (2009) modelled the dielectric loss of radar data through the ice column around Dome C in East Antarctica (Fig. 6) to infer the basal reflectivity and verify the presence of subglacial water. Because the temperature profile of the ice sheet is one parameter affecting dielectric loss, this approach required inference of the basal heat flow from temperature-depth modelling over the last 254 ka. The Shapiro and Ritzwoller (2004) GHF model was used initially (see section “4.2. Seismic estimates”), but when the calculated vertical ice velocity ( $m_w$ ) at the bed exceeded the initial melt rate ( $m_T$ ), the GHF was modified until  $m_T$  and  $m_w$  were equal. This approach identified localised high GHF anomalies, but (excepting these anomalies) they calculated that 66 % of the study area was either at or near the pressure melting point (anywhere that ice is thicker than 3500 m) without invoking enhanced GHF.

Schroeder et al. (2014) modelled the spatial distribution of melt beneath the ice sheet in the Thwaites Glacier catchment (Fig. 6) by mapping the relative bed echo strength of radar data in the region and modelling the water routing required to match these observations by routing alone (without heterogeneous basal melting). These routing models were based on the radar-derived ice thickness and surface slope. The 50 selected routing models were used to model the relative melt required to reproduce the observed echo strengths of each routing model. This relative melt model was in turn scaled to match the total melt water produced in an ice sheet model of the Thwaites Glacier incorporating frictional melting, horizontal advection, and an assumed uniform GHF. By subtracting the frictional and advective contributions, the GHF required to produce the remaining melt could be



---

Number: 1      Author: brice      Subject: Cross-Out      Date: 10/04/2020 16:16:32  
(Van Liefferinge and Pattyn, 2013).

---



---

Number: 2      Author: brice      Subject: Underline      Date: 13/04/2020 11:30:29

---

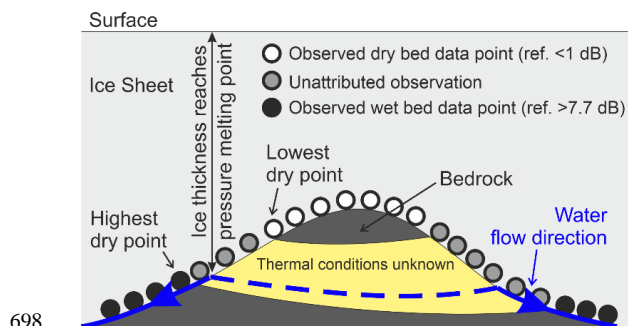
As it is difficult to know the melt rate, I would say that this is not the GHF estimate but the minimum value of the GHF estimate or the minimum GHF to reach the pressure melting point.





687 calculated. This approach predicted very high heat flow in this region (114 to  $>200 \text{ mW m}^{-2}$ ), with the highest  
 688 heat flow focused around observed and inferred subglacial volcanoes.

689 With the aim of determining appropriate sites of low basal melting for old-ice drilling, Passalacqua et al. (2017)  
 690 also used radar evidence for basal melting and ice sheet modelling to determine GHF around Dome C (Fig. 6).  
 691 Wet and dry bed conditions were identified from radar data and ten spots were identified on bedrock topographic  
 692 features marking the critical ice thickness where present basal melting becomes possible. These spots were defined  
 693 as locations where the upper slopes of the bedrock topography are dry and their lee slopes are wet, with melting  
 694 initiating between the two when the ice thickness passes the pressure melting point (Fig. 14). Assuming that GHF  
 695 is locally homogeneous between the two bedrock elevations, heat flow was determined by increasing its value in  
 696 a 1-D heat model of the local ice thickness until basal melting occurred. These point estimates were interpolated  
 697 to generate an approximate map of regional heat flow and calculate basal melt rates over the last 400 ka.








698  
 699 **Fig. 14. Illustration of how the ice thickness exceeding the pressure melting point (PMP) can be identified from radar**  
 700 **reflectivity data points, indicating the presence or absence of basal water beneath the ice sheet. Once the PMP is**  
 701 **identified, thermal modelling can estimate the required local GHF. Between the thresholds of radar reflectivities**  
 702 **representative of wet and dry basal conditions, the thermal conditions are unknown (yellow-shaded region of the**  
 703 **bedrock). Adapted from Passalacqua et al. (2017).**

704 [1]fferinge and Pattyn (2013) and [2]fferinge et al. (2018) used steady state and transient thermodynamic  
 705 modelling of the East Antarctic Ice Sheet to map the minimum heat flow required to raise the basal temperature  
 706 above pressure melting point and generate basal melting. Whilst this was executed to identify possible sites for  
 707 drilling the oldest ice in areas that are unlikely to have undergone basal melting in the last 1.5 Ma and did not  
 708 produce an estimate of absolute GHF, if this approach were combined with other evidence for basal conditions  
 709 above the pressure melting point (e.g. combining thermodynamic modelling with subglacial lake locations) [3]nts  
 710 of minimum heat flow could be mapped.

## 711 5.2. Subglacial lakes

712 If temperatures are sufficient for basal melting, and topography depressions are suitable, subglacial lakes can  
 713 develop. Subglacial lakes exhibit radio reflectivities 10-20 dB greater than the ice-bedrock boundary, allowing  
 714 the current identification of [4] lakes beneath the Antarctic ice sheet [5]

	Number: 1	Author: brice	Subject: Inserted Text	Date: 10/04/2020 16:52:15
	Van			
	Number: 2	Author: brice	Subject: Inserted Text	Date: 10/04/2020 16:52:19
	Van			
	Number: 3	Author: brice	Subject: Inserted Text	Date: 10/04/2020 17:01:02
	,			
	Number: 4	Author: brice	Subject: Inserted Text	Date: 10/04/2020 17:07:23
	more than			
	Number: 5	Author: brice	Subject: Inserted Text	Date: 10/04/2020 17:07:12
	cite: A. P. Wright and M. J. Siegert. A fourth inventory of Antarctic subglacial lakes. Antarctic Science, 24:659–664, 2012.			



Whether basal temperatures are sufficient for basal melting and preservation of subglacial lakes is dependent on ice thickness, the surface temperature and accumulation rate, heat transported through ice advection, heat produced by internal deformation and basal sliding, and the GHF. When subglacial lakes are located near ice divides, heat derived by horizontal advection, basal friction, and internal deformation is assumed to be minimal, and thus the heat required to bring the base of the ice sheet above the pressure melting point is a product of ice thickness and GHF. Thus, when subglacial lakes are located near ice divides and the accumulation rate is known (high accumulation rates cool the ice mass), point estimates of *minimum* GHF can be calculated from one-dimensional thermal models of the ice sheet temperature profile, but an assumption that water was derived locally and not routed from elsewhere must also be considered as lakes can only form in topographic depressions. The absence of a lake or basal water does not imply the bed is frozen if the water can drain away (Pattyn, 2010; Siegert and Dowdeswell, 1996).

### 5.3. Englacial stratigraphy

Jordan et al. (2018) identified draw down of internal ice sheet layers and increased bed reflectivity from radar data near the South Pole (Fig. 6), indicating enhanced basal melting. Melt rates were calculated using dated radar layers, traced from the Dome C ice-core site, and a depth age model that simulates the draw-down effect of ice from subglacial melt rate. The low ice velocity ( $<1.5 \text{ m a}^{-1}$ ) indicated minimal frictional contribution to basal temperature, and a location at the top of a hydraulic catchment area indicated a low heat contribution from subglacial water. By negating these contributions to heat flow, assuming the basal temperature is at the pressure melting point (and thus could be derived from the ice thickness) and that temporal temperature variations match those of the Dome C ice core, a time-dependent heat equation was applied to the ice sheet to derive the basal GHF required to generate the enhanced melt rates.

1

### 5.4. Microwave emissivity

Englacial temperature profiles have been derived from satellite and airborne passive detection of high frequency L-band microwave radiation ( $\sim 1.4 \text{ GHz}$ ; Macelloni et al., 2019, 2016; Passalacqua et al., 2018); data primarily collected to investigate soil moisture and ocean salinity (Kerr et al., 2010). These wavelengths have very low absorption in ice and low scattering by particles (e.g. grainsize and ice bubbles), providing high penetration depths in dry ice.

Macelloni et al. (2019) derived englacial temperature profiles for the Antarctic ice sheet from 2-year averaged vertical-polarised (V) radiation collected at the “Brewster angle” ( $57.1^\circ \pm 2.6^\circ$ ; the angle of incidence at which the radiation is perfectly transmitted through the air-snow interface with no reflection, minimising the influence of surface or shallow sub-surface effects). The corrected intensity (brightness temperature,  $T_B$ ) correlates with the surface temperature of the ice, but is also affected by the ice sheet thickness (a largely inverse correlation), density profile, and grain size (Macelloni et al., 2016). As such, the ice sheet’s thermal structure at depth could be estimated by comparing the observed  $T_B$  and a simulated  $T_B$  derived through microwave emissivity modelling, including one-dimensional modelling of the ice sheet’s temperature profile. Included in the assumed values for this modelling are the GHF and the accumulation rate; the sources of greatest uncertainty. This method only applies in areas of slow flowing ice ( $<10 \text{ m yr}^{-1}$ ), and is optimal in areas of very slow flowing ice ( $<5 \text{ m yr}^{-1}$ ) as



Number: 1      Author: brice      Subject: Inserted Text      Date: 13/04/2020 11:30:53

---

again if at the PMP, for me it is more a minimum GHF as we don't know whether there is melt or not. If the melt is low, both values are very closed to each other



752 this negates heating by horizontal ice advection and deformation-derived heat production. It is also only applicable  
753 to areas of thick ice (>1000 m) as the simulations used to model microwave emission do not include bedrock  
754 reflections. This is not a limitation for application to Antarctic GHF research, as it is under these conditions that  
755 heat flow has the greatest influence on ice sheet dynamics.

756 Comparison of the microwave-derived temperature profile and that simulated by glaciological modelling  
757 (Offeringe and Pattyn, 2013) show good agreement in the upper third of the ice sheet, but diverge in their  
758 temperature estimates with depth, with the largest uncertainties close to the bedrock. This is largely due to  
759 uncertainty in the GHF, but also reflects a decrease in sensitivity of the simulated  $T_b$  to the temperature profile  
760 below 1000-1500 m (the bottom 1000-1500 m of the ice sheet contributes <10 % to the total emission). Longer  
761 wavelength emissions (0.5 GHz) with greater sensitivity to the deeper temperature profile may provide greater  
762 accuracy at depth (Jezek et al., 2014). Deep measurements of the ice sheet's temperature profile are required to  
763 validate this method compared to the glaciological models. Although currently limited by its sensitivity to  
764 temperature at depth and the accuracy of the assumed parameters (notably accumulation rate), this approach has  
765 the potential to constrain basal heat flow through variation of the assumed GHF values used in the emissivity  
766 modelling.

## 767 6. Existing data

768 Although subglacial borehole-derived estimates of terrestrial GHF are lacking in Antarctica, estimates have been  
769 made from probes into marine sediments and boreholes into exposed bedrock. We have compiled 433 of these  
770 point estimates (Fig. 15; data available in the Supplementary Material and from  
771 <https://github.com/RicardaDziadek/Antarctic-GHF-DB>). However, the compiled data originates from multiple  
772 methods, and is variable in its accuracy and limitations. We do not include values for marine measurements  
773 compiled in the database "Global Heat Flow Data – Abbott Compilation". This database is available via  
774 GeoMapApp and completely undocumented. The labels may point to cruise reports, but not published data and  
775 the data quality remains impossible to evaluate up to this point.



Van

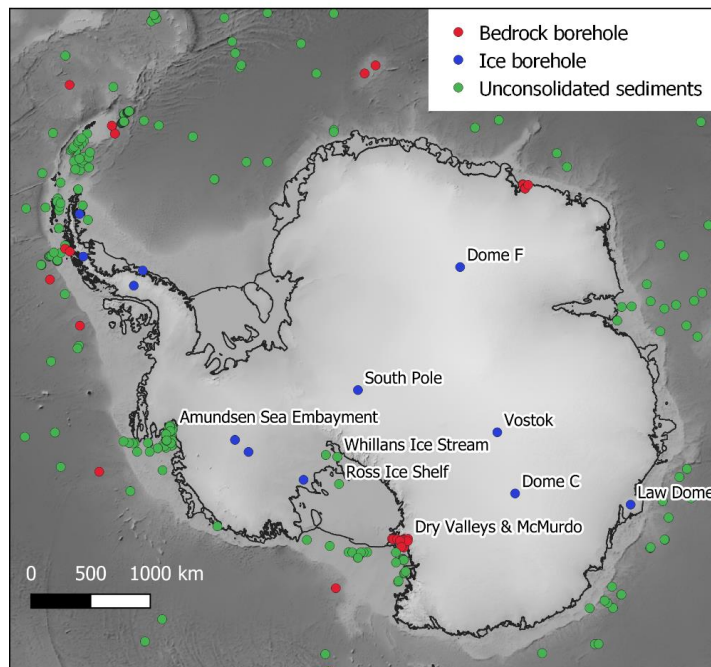


**Fig. 15. Locations of all compiled point estimates of GHF. Database available in the Supplementary Material and from <https://github.com/RicardaDziadek/Antarctic-GHF-DB>.**

### 6.1. Boreholes into bedrock

Terrestrial, borehole-derived measurements of the geothermal gradient are limited to the Dry Valleys and McMurdo Sound region (Fig. 15; Bucher, 1980; Decker, 1974; Decker and Bucher, 1982; Pruss et al., 1974; Talalay and Pyne, 2017), and no subglacial terrestrial borehole measurements have been made into the Antarctic bedrock. However, as discussed in Section 3.1., temperature gradients in bedrock must be taken to a sufficient depth to be representative of upward conduction of the GHF rather than downward conduction of the surface temperature. Whilst the GHF estimates from the Dry Valleys Drilling Project (DVDP, including McMurdo Station) were taken from the 75 to >300 m deep boreholes (Bucher, 1980; Decker and Bucher, 1982; Talalay and Pyne, 2017), the shallow 7.6 m borehole from McMurdo Station produces a much higher GHF estimate ( $164 \text{ mW m}^{-2}$ , Risk and Hochstein, 1974). This shallow measurement should thus be neglected in preference for the  $66 \text{ mW m}^{-2}$  value from the 260 m deep DVDP borehole (Decker and Bucher, 1982).

Boreholes into submarine bedrock have been drilled and temperature gradients measured beneath the McMurdo Sound, Amundsen Sea Embayment, and Ross Ice Shelf (Fig. 15; Bückner et al., 2001; Decker et al., 1975; Gohl et al., 2019; McKay et al., 2018; Morin et al., 2010).

The US Rapid Access Ice Drill project (RAID) aims to achieve the first subglacial, borehole-derived thermal measurements of bedrock following drilling of the overlying ice sheet and coring of  $\geq 25 \text{ m}$  of bedrock (Goode and Severinghaus, 2016).

This page contains no comments





## 6.2. Ice boreholes<sup>1</sup>

GHF estimates from ice boreholes are better distributed across the Antarctic continent than terrestrial bedrock boreholes (Fig. 15). However, not all ice boreholes drilled have been sufficiently deep or in appropriate sites for GHF estimation (i.e. the ice sheet needs to be stationary and frozen to the bed). This limits the available GHF estimates to Vostok (Salamat et al., 1998), Dome Fuji (Hondoh et al., 2002), Law Dome (Dahl-Jensen et al., 1999), South Pole (Price et al., 2002), Marie Byrd Land (Clow et al., 2012; Engelhardt, 2004; Gow et al., 1968), and the Antarctic Peninsula (Mulvaney et al., 2012; Nicholls and Paren, 1993; Zagorodnov et al., 2012) (Fig. 15).

## 6.3. Marine and onshore unconsolidated sediments

The most abundant resource of heat flow estimates from measured temperature profiles around Antarctica comes from unconsolidated marine sediments (Fig. 15). However, the data distribution is sparse and heterogeneous, and whilst some regions are well sampled (e.g. the Amundsen Sea embayment; Dziadek et al., 2019, 2017), other regions (e.g. the Weddell Sea) remain poorly constrained (Fig. 15). In addition to the open water measurements, two shallow probes (deepest sensors at 1.4 and 0.8 m below the upper sediment surface) have measured the temperature gradient in subglacial sediments below the Whillans Ice Stream (Begeman et al., 2017; Fisher et al., 2015; see section 3.3.). Two temperature gradients have also been measured beneath the Ross Ice Shelf (Foster, 1978; Morin et al., 2010), but otherwise heat flow beneath the Antarctic ice shelves remains poorly constrained regions.




As discussed in Section 3.3, when using these estimates it is important to consider whether the shallow (<~5 m) temperature gradient recorded by the probe is representative of the deeper GHF, or will have been perturbed by temperature variation in the overlying ice sheet or water column (e.g. Dziadek et al., 2019). Consequently, the water depth, the temperature profile of the water column, and possible sources of long-term temperature variation (e.g. variations in deep water circulation and temperature) should be considered when selecting appropriate point estimates. Similarly, whilst the shallow temperature gradients measured from Subglacial Lake Whillans (Fisher et al., 2015), and the Whillans Ice Stream grounding zone (Begeman et al., 2017) are presented as subglacial direct measurements of Antarctic GHF, by the nature of their location within an ice stream they are not in a thermal steady state, and the temperature profile will have been affected by long term variation from heat advection and shear heating. These are effects that cannot be evaluated from their very shallow temperature gradient (0.8 and 1.4 m deep), and accordingly these estimates should be used with caution.

## 7. Current challenges and future research directions<sup>3</sup>

The collated existing data and methodologies presented above highlight our current limitations in determining the subglacial GHF of Antarctica and allow discussion of future research.

### 7.1. Borehole and probe-derived estimates

The fundamental limitation for GHF estimation in Antarctica is the lack of borehole-derived estimates from beneath the Antarctic ice sheet. Without these independent, discrete validation points, the more extensive regional estimates cannot be accurately evaluated. Therefore, the most promising future development will be the  $\geq 25$  m deep bedrock borehole measurements of the Rapid Access Ice Drill project (RAID; Goodge and Severinghaus,

- 
-  Number: 1      Author: brice      Subject: Inserted Text      Date: 10/04/2020 17:18:13  
You should include the new TCD paper of Talalay 2020: <https://www.the-cryosphere-discuss.net/tc-2020-32/tc-2020-32.pdf>
- 
-  Number: 2      Author: brice      Subject: Underline      Date: 10/04/2020 17:19:47  
Dome Fuji is not frozen to the bed, so it is a minimum GHF
- 
-  Number: 3      Author: brice      Subject: Inserted Text      Date: 13/04/2020 11:31:34  
I strongly suggest to add a few words on machine learning techniques as done in Greenland by Rezvanbehbahani et al. (2017). See before and something like: "Machine learning techniques used to determine the GHF over the Greenland Ice Sheet (Rezvanbehbahani et al., 2017) could be developed for the Antarctic Ice sheet. Up until now, we provide a statistical analysis of basal temperatures and GHF based on the use of different data sets. The use of a Monte Carlo approach, which is based on repeated random sampling to calculate GHF, could bring new perspectives on the data, and in particular on associated uncertainties which would allow us to critically assess our results."

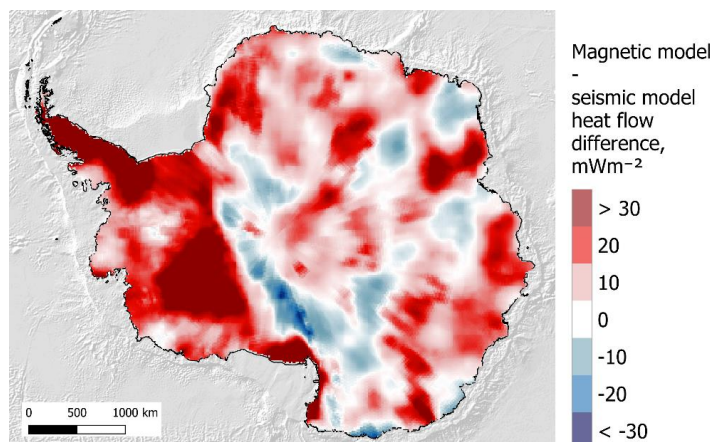


2016). However, (as noted above) local temperature gradients may not be representative of the regional heat flow, as local geology, hydrothermal circulation, and topography can result in localised GHF variability. In response, multiple boreholes are required to categorise the regional variation, and topographic effects must be considered and accounted for.

It is also a necessity that thermal modelling of the bedrock temperature profile for the RAID target sites is executed prior to drilling to constrain the penetration depth of low-frequency time variation of temperature. Whilst the RAID target bedrock borehole depth of  $\geq 25$  m is much shallower than the  $>100$  m borehole depth achieved for exposed bedrock (Section 3.1.), the overlying ice sheet insulates the bedrock temperature profile from short duration surface temperature variability (temperature variation penetration depth is dependent on the frequency of the variation and thermal diffusivity of the material; Carslaw and Jaeger, 1959). However, as is considered for GHF estimates from ice boreholes (Section 3.2.), low-frequency variation in surface temperatures, heat advection, and shear heating will all affect the subglacial temperature profile. Consequently, low-frequency temperature variation must be corrected for, and boreholes are best drilled where the ice is stationary and frozen to the bed (as is applied to ice borehole selection for GHF estimation). By drilling in such sites where glaciological approaches are most effective for GHF estimation, the RAID data will allow validation of GHF estimates for the various englacial temperature methods applied to stationary ice at ice divides (Section 5.). These methods include borehole temperature profiles, subglacial lakes, ice sheet models, and microwave emissivity. It is thus important that the englacial temperature profile is measured in addition to the bedrock temperature gradient.

Beyond bedrock drilling there is lot to be gained from further ice borehole drilling. Firstly, existing data must be evaluated to ensure the methodologies of GHF modelling from borehole temperature profiles are consistent and accurate. This is particularly true for the Dome C borehole, for which the previously published  $49.0 \text{ mW m}^{-2}$  value (de Mendoza et al., 2016) has been retracted. Future ice boreholes into stationary ice frozen to the bed has the potential to supplement the existing borehole and probe-derived GHF estimates, particularly if the proposed methodology for shallow boreholes can be validated (600 m depth, or the upper 20% of the ice column; Section 3.2.).

## 7.2. Geophysical GHF estimates





and only where the bed is frozen.



859 **Fig. 16. Difference in heat flow values between the most recent magnetic (Martos et al., 2017) and seismic (An et al.,**  
 860 **2015b) heat flow models.**

861 Whilst only geophysical methods have provided continental-scale GHF estimates, their values and distribution  
 862 vary greatly (Fig. 5 and Fig. 16). Uncertainties of  $<10 \text{ mW m}^{-2}$  for the majority of Antarctica were presented for  
 863 the Curie Depth GHF model of Martos et al. (2017). However, not only are the modelled values greatly different  
 864 from those derived by seismic modelling (An et al., 2015b), the calculated Curie depth is deeper than the  
 865 seismically- or gravitationally-derived Moho depth for large areas of the continent (Fig. 10). Whilst this can occur  
 866 where metallic phases are present in cratonic mantle (Ferré et al., 2013; Section 4.1.), this cannot explain the full  
 867 distribution, nor are these occurrences likely to be this extensive. Without being critical of the model itself, it is  
 868 reasonable to dispute the accuracy of the calculated uncertainties, and suggest that whilst their calculation from  
 869 the geophysical data may be logical, there may be a geological contribution to uncertainty (e.g. lithological  
 870 variation in the lithosphere) that is not being considered. As GHF models are utilised by researchers in different  
 871 fields to those publishing the models, they cannot be independently evaluated by the user, and so accuracy in  
 872 published uncertainty values is arguably more important than the accuracy of the model itself. We recommend  
 873 that future research (including geophysical, geological, glaciological, and borehole and probe-derived estimates)  
 874 is careful in its presentation of uncertainty.

875 The largest limitations to existing geophysical-derived GHF models are uncertainties in the structure,  
 876 composition, heat production, and thermophysical properties of the unexposed crust, lithosphere, and underlying  
 877 mantle. All current continental models assume the lithosphere to be laterally homogenous in its composition and  
 878 thermophysical properties, and although seismic GHF models (e.g. An et al., 2015b) incorporate variable mantle  
 879 temperatures, its composition is assumed to be homogenous. Geophysical GHF models assume that lithospheric  
 880 heat production is focussed in the upper crust, and is orders of magnitude greater than the deeper heat production  
 881 of the middle and lower crust and the mantle. These models assume that lithospheric heat production either  
 882 exponentially decreases with depth (e.g. the Curie depth models of Fox Maule et al., 2005, and Martos et al.,  
 883 2017) or is concentrated within a laterally homogenous layer of variable depth and constant heat production (e.g.  
 884 the seismic model of An et al., 2015a, and the thermal-isostatic model for Australia of Hasterok and Gard, 2016).  
 885 However, although the lower crust is enriched in mafic rocks (iron-rich rocks of high crystallisation temperature,  
 886 e.g. basalt) of low heat production, deep boreholes and crustal sections have shown that whilst there is a correlation  
 887 between heat production and lithology in the upper crust, there is no such correlation with depth or metamorphic  
 888 grade (Section Section 4.6.3.). Similarly, the assumption of laterally homogenous heat production has been shown  
 889 to be unreasonable for estimation of Antarctica's GHF, which (like all continents) has a laterally variable geology  
 890 and associated concentration of HPEs (Burton-Johnson et al., 2017; Carson et al., 2014). The exponential decrease  
 891 model of crustal heat production should thus be rejected, and attempts should be made to derive the depth and  
 892 structure of crustal heat production.

893 The most promising approach to address the challenge of uncertainty in the contribution to GHF from the  
 894 unexposed crust and deeper lithosphere is the derivation of a three-dimensional lithospheric structure model for  
 895 Antarctica. This approach uses geophysical modelling integrating seismic, magnetic, and thermal-isostatic  
 896 evidence, and integrating into the modelling the heat production, conductivity, and petrophysical properties of  
 897 exposed lithologies and deeper crustal xenoliths or crustal sections. A similar model was developed for Norway

This page contains no comments



898 (Ebbing et al., 2006; Olesen et al., 2007), and an Antarctic model would build upon recent 2D and 3D  
899 geophysically-derived models (Leat et al., 2018; Pappa et al., 2019b, 2019a). Beneath the Antarctic ice sheet,  
900 where the surface geology is unknown, the lithologies and probable heat production is best constrained by  
901 determining the probable heat production of each drainage basin based on its detrital clasts (e.g. Goodge, 2018).

902 The assumption of a homogenous mantle composition beneath East Antarctica is challenged by discrepancies  
903 between the Moho depth models derived by gravity and isostatic modelling (Pappa et al., 2019b, 2019a), as this  
904 indicates variable lithospheric mantle densities, or deeper mantle effects on topography. A review of the available  
905 mantle xenoliths and mantle-derived basalt chemistry may be able to constrain the composition of the mantle  
906 beneath Antarctica, and thermal-isostatic modelling may be able to identify these regions of anomalous mantle  
907 anomalies (as in the Australian study of Hasterok and Gard, 2016). If the seismic data for Antarctica is sufficient  
908 to determine crustal density, such a thermal isostatic model would provide an additional independent method to  
909 determine the depth of the upper crustal heat producing layer (Hasterok and Chapman, 2011) and evaluate the  
910 other GHF models.

911 Finally, it is important to compare Antarctica with its conjugate margins (e.g. Pollett et al., 2019), where GHF and  
912 crustal structure are better constrained. This provides constraints on the GHF along the margins of East Antarctica,  
913 as well as informing on the geology beneath the ice sheet.

### 914 7.3. Glaciological GHF estimates

915 Englacial temperatures are more sensitive to GHF in areas of the interior of Antarctica where basal sliding is  
916 negligible (Section 2.1). Out of all the methods discussed to derive GHF in the Antarctic interior, the most  
917 promising method is to derive GHF from englacial temperatures obtained from microwave emission (Section 5.4.)  
918 at a longer wavelength (0.5 GHz) than the currently available (~1.4 GHz). The increase in wavelength will reduce  
919 the uncertainty in englacial temperatures below 1000-1500 m (Jezek et al., 2014). By improving the estimations  
920 of englacial temperature near the bed, this will reduce the role of ice flow modelling required to extrapolate  
921 temperature from the partial-depth data. Potentially, if near-the-bed englacial temperatures are known with  
922 sufficient precision, GHF could be derived as from borehole thermometry (Section 3.2). However, this method  
923 requires the acquisition of currently unavailable satellite-derived data as, despite the potential of this method, the  
924 2018 Cryorad proposal submitted to ESA (Macelloni et al., 2018) was unsuccessful.

925 Existing glaciological data, like subglacial water distribution or dated englacial layers, has been successfully used  
926 in estimating heat flow in regions of thick, slow flowing ice near ice divides, where advection and shear heating  
927 are minimised. To extend these regional studies to continental scale, both data and models have to be improved.  
928 A significant challenge for radar-derived subglacial water distribution is our ability to discriminate between water  
929 at the bed versus contrasts in the geometric properties of ice sheet and bed (Schroeder et al., 2014). However the  
930 improvement in radar techniques and the combination with seismic surveys and direct access observations, is our  
931 best chance to improve our observations of subglacial hydrology (Ashmore and Bingham, 2014).

932 The inventory of subglacial lakes (Wright and Siegert, 2012) is a better constrained and expanding dataset.  
933 Subglacial lakes can be detected also using satellite surface altimetry (Fricker et al., 2007), providing a way to  
934 expand the coverage and to confirm dubious cases. However, as noted in Section 5.1., topography must be

This page contains no comments





935 considered when using evidence for subglacial lakes as they can only develop in topographic depressions, and the  
936 absence of basal water does not imply the bed is frozen if water can drain away.

937 Subglacial melting can also be detected in englacial stratigraphy (Section 5.3) but the required radar product  
938 (internal radar reflective horizons) is not often available. “AntArchitecture” is a SCAR (Scientific Committee on  
939 Antarctic Research) Action Group bringing together key datasets on Antarctic internal layering from the principal  
940 institutions and scientists who have been responsible for acquiring, processing and storing them over the last four  
941 decades (AntArchitecture Action Group, 2017). As the coverage of Antarctic internal layers becomes widely  
942 available, its application to infer GHF will increase in popularity.

943 Finally, and for any of the glaciological methods described above, the glaciological models used to infer GHF  
944 have to be improved. The current thermal models used to infer GHF can be classified in two larger groups: 1) 1D  
945 time-dependent high-complexity models, and 2) 2D/3D steady-state low-complexity models. The first category is  
946 generally used near ice domes or ridges, with low horizontal flow, and where horizontal heat advection can be  
947 neglected (e.g., Passalacqua, 2017). The latter are used across the whole continent (e.g., <sup>1</sup>Jeffering, 2018), but  
948 ignore the changes in temperature between glacial and interglacial periods despite their strong effect on englacial  
949 temperatures (Ritz, 1989). The challenge is to develop thermal models with the required level of complexity at a  
950 continental scale, accommodating the main physical processes. This remains a technical challenge.<sup>2</sup>

## 951 8. Conclusions




952 We present state-of-the-art data and models to estimate geothermal heat flow in Antarctica and highlight the need  
953 for a detailed continental map. We also discuss current challenges and future directions.

954 With multiple methodologies and models for Antarctic GHF currently published, the most promising future  
955 direction<sup>3</sup> is borehole-derived estimation of GHF beneath the Antarctic ice sheet from RAID bedrock drilling and  
956 englacial temperatures from ice boreholes. Ideally, the latter approach will be validated by the former to support  
957 expansion of the dataset from shallow boreholes (potentially only 600 m deep, or 20 % of the total ice sheet  
958 thickness).

959 The ice sheet is most sensitive to variation in GHF within the interior of Antarctica, where heat production from  
960 slide at the base of the ice sheet is negligible. However, it is in this region that GHF is hardest to constrain by  
961 geophysical estimates because of the scarcity of local GHF estimates from down-hole measured temperature  
962 gradients, geological data, and insight from conjugate margins. It is thus in the interior of Antarctica where  
963 glaciological approaches are the most applicable. Out of the methods presented, the determination of englacial  
964 temperatures from long-wavelength microwave emissivity is the most promising, but this data is not currently  
965 available.

966 We highlight the potential of regional estimates of GHF from subglacial meltwater inventories. Aside from the  
967 ever expanding inventory of subglacial lakes we encourage initiatives like “AntAntarctica” that will make radar  
968 products widely available. Also, we discuss future requirements of thermal models (either 1D or those lacking  
969 glacial-interglacial variability) to expand the methods beyond domes in the interior of Antarctica.

---

	Number: 1	Author: brice	Subject: Inserted Text	Date: 10/04/2020 17:43:12
Van				
	Number: 2	Author: brice	Subject: Inserted Text	Date: 13/04/2020 11:31:51
I would add that up until now, thermodynamical models are still dependent of GHF estimates (large GHF data sets, borehole temperature measurements, ...)				
	Number: 3	Author: brice	Subject: Inserted Text	Date: 13/04/2020 10:13:28
for local measurements				

---



970 Geophysical methods remain the most attractive approach to estimate GHF because they are independent of ice  
 971 flow. However, they vary greatly in their estimated magnitude and distribution of GHF. The greatest uncertainty  
 972 in all the geophysical models is uncertainty in the composition and structure of the lithosphere and mantle. We  
 973 recommend ceasing to use the exponential decrease model of crustal heat production. Instead, we suggest using  
 974 geological and geophysical approaches to model the thickness, structure and composition of the crust. We also  
 975 recommend the application of a thermal-isostatic approach to provide an independent estimate, and highlight  
 976 regions of anomalous isostatic elevation and probable mantle heterogeneities.

977 Finally, the greatest challenge for Antarctic GHF estimation is the necessity for multidisciplinary science.  
 978 Hopefully, this paper provides a first step in communicating the approaches and limitations of the different fields  
 979 across the GHF community. We sincerely recommend the continuation and enhancement of the international  
 980 collaborations within SCAR, building on the work of the GHF sub-group of the SERCE research programme  
 981 (Solid Earth Response and influence on Cryospheric Evolution), and encourage and appreciate SCAR's  
 982 continuing support in this field of research.

## 983 **9. Acknowledgements**

984 A. Burton-Johnson and C. Martin were funded by the Natural Environment Research Council as part of the British  
 985 Antarctic Survey Polar Science for Planet Earth programme. R. Dziadek was supported by the Deutsche  
 986 Forschungsgemeinschaft (DFG) in the framework of the Priority Program 1158 “Antarctic research with  
 987 comparative investigations in Arctic ice areas” by grant GO 724/14-1. Additional funds were contributed by the  
 988 AWI Research Program PACES-II Workpackage 3.2. This research is a contribution to the SCAR SERCE  
 989 programme, and we thank the discussions and support of this group from the TACTical 2018 (Hobart, Australia),  
 990 POLAR 2018 (Davos, Switzerland), and ISAES 2019 (Incheon, Korea) meetings. We particularly thank  
 991 Jacqueline Halpin (IMAS) for her comments on the manuscript and her in work promoting and developing the  
 992 Antarctic GHF community.

## 993 **10. References**

- 994 Aboud, E., Salem, A. and Mekkawi, M.: Curie depth map for Sinai Peninsula, Egypt deduced from the analysis  
 995 of magnetic data, *Tectonophysics*, 506(1–4), 46–54, 2011.
- 996 Aitken, A. R. A., Betts, P. G., Young, D. A., Blankenship, D. D., Roberts, J. L. and Siegert, M. J.: The Australo-  
 997 Antarctic Columbia to Gondwana transition, *Gondwana Research*, 29(1), 136–152, 2016.
- 998 Alessio, K. L., Hand, M., Kelsey, D. E., Williams, M. A., Morrissey, L. J. and Barovich, K.: Conservation of deep  
 999 crustal heat production, *Geology*, 46(4), 335–338, 2018.
- 1000 Amante, C. and Eakins, B. W.: ETOPO1 Arc-Minute Global Relief Model: Procedures, Data Sources and  
 1001 Analysis, National Oceanic and Atmospheric Administration Technical Memorandum NESDIS NGDC-24., 2009.
- 1002 An, M., Wiens, D. A., Zhao, Y., Feng, M., Nyblade, A. A., Kanao, M., Li, Y., Maggi, A. and L  v  que, J.-J.: S-  
 1003 velocity model and inferred Moho topography beneath the Antarctic Plate from Rayleigh waves, *Journal of*  
 1004 *Geophysical Research: Solid Earth*, 120(1), 359–383, 2015a.
- 1005 An, M., Wiens, D. A., Zhao, Y., Feng, M., Nyblade, A., Kanao, M., Li, Y., Maggi, A. and L  v  que, J.-J.:  
 1006 Temperature, lithosphere-asthenosphere boundary, and heat flux beneath the Antarctic Plate inferred from seismic  
 1007 velocities, *Journal of Geophysical Research: Solid Earth*, 120(12), 8720–8742, 2015b.

This page contains no comments



- 1008 Andrés, J., Marzán, I., Ayarza, P., Martí, D., Palomeras, I., Torné, M., Campbell, S. and Carbonell, R.: Curie point  
1009 depth of the Iberian Peninsula and surrounding margins. A thermal and tectonic perspective of its evolution,  
1010 *Journal of Geophysical Research: Solid Earth*, 123(3), 2049–2068, 2018.
- 1011 AntArchitecture Action Group: AntArchitecture: Archiving and interrogating Antarctica's internal structure from  
1012 radar sounding. Final Report, University of Edinburgh, UK. [online] Available from:  
1013 <https://www.scar.org/library/science-4/geosciences/antarchitecture/5240-antarchitecture-workshop-2017/file>,  
1014 2017.
- 1015 Arnaiz-Rodríguez, M. S. and Orihuela, N.: Curie point depth in Venezuela and the Eastern Caribbean,  
1016 *Tectonophysics*, 590, 38–51, 2013.
- 1017 Artemieva, I.: *Lithosphere: an interdisciplinary approach*, Cambridge University Press, Cambridge, UK., 2011.
- 1018 Artemieva, I. M. and Mooney, W. D.: Thermal thickness and evolution of Precambrian lithosphere: A global  
1019 study, *Journal of Geophysical Research: Solid Earth*, 106(B8), 16387–16414, 2001.
- 1020 Ashmore, D. W. and Bingham, R. G.: Antarctic subglacial hydrology: current knowledge and future challenges,  
1021 *Antarctic Science*, 26(6), 758–773, 2014.
- 1022 Bansal, A. R., Gabriel, G., Dimri, V. P. and Krawczyk, C. M.: Estimation of depth to the bottom of magnetic  
1023 sources by a modified centroid method for fractal distribution of sources: An application to aeromagnetic data in  
1024 Germany, *Geophysics*, 76(3), L11–L22, 2011.
- 1025 Bansal, A. R., Anand, S. P., Rajaram, M., Rao, V. K. and Dimri, V. P.: Depth to the bottom of magnetic sources  
1026 (DBMS) from aeromagnetic data of Central India using modified centroid method for fractal distribution of  
1027 sources, *Tectonophysics*, 603, 155–161, 2013.
- 1028 Barletta, V. R., Bevis, M., Smith, B. E., Wilson, T., Brown, A., Bordoni, A., Willis, M., Khan, S. A., Rovira-  
1029 Navarro, M. and Dalziel, I.: Observed rapid bedrock uplift in Amundsen Sea Embayment promotes ice-sheet  
1030 stability, *Science*, 360(6395), 1335–1339, 2018.
- 1031 Baron Fourier, J. B. J.: *Théorie analytique de la chaleur*, Chez Firmin Didot, père et fils, Paris., 1822.
- 1032 Barrett, B. E., Nicholls, K. W., Murray, T., Smith, A. M. and Vaughan, D. G.: Rapid recent warming on Rutford  
1033 Ice Stream, West Antarctica, from borehole thermometry, *Geophysical Research Letters*, 36(2) [online] Available  
1034 from: <http://onlinelibrary.wiley.com/doi/10.1029/2008GL036369/full> (Accessed 22 March 2017), 2009.
- 1035 Bea, F.: The sources of energy for crustal melting and the geochemistry of heat-producing elements, *Lithos*, 153,  
1036 278–291, doi:10.1016/j.lithos.2012.01.017, 2012.
- 1037 Bea, F. and Montero, P.: Behavior of accessory phases and redistribution of Zr, REE, Y, Th, and U during  
1038 metamorphism and partial melting of metapelites in the lower crust: an example from the Kinzigite Formation of  
1039 Ivrea-Verbano, NW Italy, *Geochimica et Cosmochimica Acta*, 63(7), 1133–1153, 1999.
- 1040 Beamish, D. and Busby, J.: The Cornubian geothermal province: heat production and flow in SW England:  
1041 estimates from boreholes and airborne gamma-ray measurements, *Geothermal Energy*, 4(1), 4, 2016.
- 1042 Beardsmore, G. R. and Cull, J. P.: *Crustal heat flow: a guide to measurement and modelling*, Cambridge  
1043 University Press, Cambridge, UK., 2001.
- 1044 Begeman, C. B., Tulaczyk, S. M. and Fisher, A. T.: Spatially variable geothermal heat flux in West Antarctica:  
1045 evidence and implications, *Geophysical Research Letters*, 44(19), 9823–9832, 2017.
- 1046 Berg, J. H., Moscati, R. J. and Herz, D. L.: A petrologic geotherm from a continental rift in Antarctica, *Earth and  
1047 Planetary Science Letters*, 93(1), 98–108, 1989.

This page contains no comments



- 1048 Bhattacharyya, B. K. and Leu, L.-K.: Analysis of magnetic anomalies over Yellowstone National Park: mapping  
 1049 of Curie point isothermal surface for geothermal reconnaissance, *Journal of Geophysical Research*, 80(32), 4461–  
 1050 4465, 1975.
- 1051 Blakely, R. J.: *Potential theory in gravity and magnetic applications*, Cambridge university press, Cambridge,  
 1052 UK., 1996.
- 1053 Blakely, R. J., Brocher, T. M. and Wells, R. E.: Subduction-zone magnetic anomalies and implications for  
 1054 hydrated forearc mantle, *Geology*, 33(6), 445–448, 2005.
- 1055 Boden, D. R.: *Geology and Heat Architecture of the Earth's Interior*, in *Geologic Fundamentals of Geothermal*  
 1056 *Energy*, Routledge., 2016.
- 1057 Bodorkos, S., Sandiford, M., Minty, B. R. and Blewett, R. S.: A high-resolution, calibrated airborne radiometric  
 1058 dataset applied to the estimation of crustal heat production in the Archaean northern Pilbara Craton, Western  
 1059 Australia, *Precambrian Research*, 128(1–2), 57–82, 2004.
- 1060 Bucher, G. J.: *Heat flow and radioactivity studies in the Ross Island-Dry Valley area, Antarctica and their tectonic*  
 1061 *implications.*, PhD Thesis, University of Wyoming, Wyoming, USA., 1980.
- 1062 Bücker, C., Jarrard, R. D. and Wonik, T.: Downhole temperature, radiogenic heat production, and heat flow from  
 1063 the CRP-3 drillhole, Victoria Land Basin, Antarctica, *Terra Antarctica*, 8(3), 151–160, 2001.
- 1064 Bullard, E. C.: The disturbance of the temperature gradient in the earth's crust by inequalities of height,  
 1065 *Geophysical Supplements to the Monthly Notices of the Royal Astronomical Society*, 4(5), 360–362, 1938.
- 1066 Bullard, E. C.: The time taken for a borehole to attain temperature equilibrium, *Monthly Notices of the Royal*  
 1067 *Astronomical Society, Geophysics Supplement*, 5, 127–130, 1947.
- 1068 Burton-Johnson, A., Halpin, J. A., Whittaker, J. M., Graham, F. S. and Watson, S. J.: A new heat flux model for  
 1069 the Antarctic Peninsula incorporating spatially variable upper crustal radiogenic heat production, *Geophysical*  
 1070 *Research Letters*, 44(11), 5436–5446, doi:10.1002/2017GL073596, 2017.
- 1071 Burton-Johnson, A., Dziadek, R. and Shen, W.: Report of the Geothermal Heat Flux Side Meeting at XIII ISAES,  
 1072 2019, Incheon, Republic of Korea. [online] Available from: [https://www.scar.org/scar-library/search/science-](https://www.scar.org/scar-library/search/science-4/research-programmes/serce/5334-ghf-meeting-report-2019/file)  
 1073 [4/research-programmes/serce/5334-ghf-meeting-report-2019/file](https://www.scar.org/scar-library/search/science-4/research-programmes/serce/5334-ghf-meeting-report-2019/file), 2019.
- 1074 Carlson, R. W., Pearson, D. G. and James, D. E.: Physical, chemical and chronological characteristics of  
 1075 continental mantle, *Reviews in Geophysics*, 43, RG1001, doi:10.1029/2004RG000156, 2005.
- 1076 Carslaw, H. S. and Jaeger, J. C.: *Conduction of heat in solids*, Oxford: Clarendon Press, 1959, 2nd ed., 1959.
- 1077 Carson, C. J. and Pittard, M.: *A Reconnaissance Crustal Heat Production Assessment of the Australian Antarctic*  
 1078 *Territory (AAT)*, Geoscience Australia, Canberra, Australia., 2012.
- 1079 Carson, C. J., McLaren, S., Roberts, J. L., Boger, S. D. and Blankenship, D. D.: Hot rocks in a cold place: high  
 1080 sub-glacial heat flow in East Antarctica, *Journal of the Geological Society*, 171(1), 9–12, 2014.
- 1081 Carter, S. P., Blankenship, D. D., Young, D. A. and Holt, J. W.: Using radar-sounding data to identify the  
 1082 distribution and sources of subglacial water: application to Dome C, East Antarctica, *Journal of Glaciology*,  
 1083 55(194), 1025–1040, 2009.
- 1084 Chen, B., Haeger, C., Kaban, M. K. and Petrunin, A. G.: Variations of the effective elastic thickness reveal tectonic  
 1085 fragmentation of the Antarctic lithosphere, *Tectonophysics*, 746, 412–424, 2018.
- 1086 Clauser, C., Giese, P., Huenges, E., Kohl, T., Lehmann, H., Rybach, L., Šafanda, J., Wilhelm, H., Windloff, K.  
 1087 and Zoth, G.: The thermal regime of the crystalline continental crust: implications from the KTB, *Journal of*  
 1088 *Geophysical Research: Solid Earth*, 102(B8), 18417–18441, 1997.

This page contains no comments

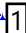




- 1089 Clow, G. D., Cuffey, K. M. and Waddington, E. D.: High heat-flow beneath the central portion of the West  
1090 Antarctic Ice Sheet, in AGU Fall Meeting Abstracts., 2012.
- 1091 Courtney, R. C. and White, R. S.: Anomalous heat flow and geoid across the Cape Verde Rise: evidence for  
1092 dynamic support from a thermal plume in the mantle, *Geophysical Journal International*, 87(3), 815–867, 1986.
- 1093 Cuffey, K. M. and Paterson, W. S. B.: *The physics of glaciers*, Academic Press., 2010.
- 1094 Cuffey, K. M., Clow, G. D., Alley, R. B., Stuiver, M., Waddington, E. D. and Saltus, R. W.: Large arctic  
1095 temperature change at the Wisconsin-Holocene glacial transition, *Science*, 270(5235), 455–458, 1995.
- 1096 Daczko, N. R., Halpin, J. A., Fitzsimons, I. C. and Whittaker, J. M.: A cryptic Gondwana-forming orogen located  
1097 in Antarctica, *Scientific reports*, 8(1), 8371, 2018.
- 1098 Dahl-Jensen, D., Morgan, V. I. and Elcheikh, A.: Monte Carlo inverse modelling of the Law Dome (Antarctica)  
1099 temperature profile, *Annals of Glaciology*, 29, 145–150, 1999.
- 1100 Dalby, C. J., Shail, R. K., Batchelor, A., Cotton, L., Gutmanis, J., Rollinson, G. K., Wall, F. and Hickey, J.: Deep  
1101 geothermal energy from the Cornubian Batholith: preliminary lithological and heat flow insights from the United  
1102 Downs Deep Geothermal Power Project, Plymouth, UK., 2020.
- 1103 Decker, E. R.: Preliminary geothermal studies of the Dry Valley Drilling Project holes at McMurdo Station, Lake  
1104 Vanda, Lake Vida, and New Harbor, Antarctica, *Bulletin-Dry Valley Drilling Project (DVDP)*, 4, 22–23, 1974.
- 1105 Decker, E. R. and Bucher, G. J.: Geothermal studies in the Ross Island-Dry Valley region, *Antarct Geosci*, 4, 887–  
1106 894, 1982.
- 1107 Decker, E. R., Baker, K. H. and Harris, H.: Geothermal studies in the Dry Valleys and on Ross Island, *Antarctic  
1108 Journal*, 10(4), 176, 1975.
- 1109 Dyment, J. and Arkani-Hamed, J.: Equivalent source magnetic dipoles revisited, *Geophysical Research Letters*,  
1110 25(11), 2003–2006, 1998.
- 1111 Dziadek, R., Gohl, K., Diehl, A. and Kaul, N.: Geothermal heat flux in the Amundsen Sea sector of West  
1112 Antarctica: New insights from temperature measurements, depth to the bottom of the magnetic source estimation,  
1113 and thermal modeling, *Geochemistry, Geophysics, Geosystems*, 18(7), 2657–2672, 2017.
- 1114 Dziadek, R., Gohl, K. and Kaul, N.: Elevated geothermal surface heat flow in the Amundsen Sea Embayment,  
1115 West Antarctica, *Earth and Planetary Science Letters*, 506, 530–539, 2019.
- 1116 Ebbing, J., Lundin, E., Olesen, O. and Hansen, E. K.: The mid-Norwegian margin: a discussion of crustal  
1117 lineaments, mafic intrusions, and remnants of the Caledonian root by 3D density modelling and structural  
1118 interpretation, *Journal of the Geological Society*, 163(1), 47–59, 2006.
- 1119 Elbeze, A. C.: On the existence of another source of heat production for the earth and planets, and its connection  
1120 with gravitomagnetism, *SpringerPlus*, 2(1), 1–13, doi:10.1186/2193-1801-2-513, 2013.
- 1121 Engelhardt, H.: Ice temperature and high geothermal flux at Siple Dome, West Antarctica, from borehole  
1122 measurements, *Journal of Glaciology*, 50(169), 251–256, 2004.
- 1123 Fahnestock, M., Abdalati, W., Joughin, I., Brozena, J. and Gogineni, P.: High geothermal heat flow, basal melt,  
1124 and the origin of rapid ice flow in central Greenland, *Science*, 294(5550), 2338–2342, 2001.
- 1125 Ferraccioli, F., Finn, C. A., Jordan, T. A., Bell, R. E., Anderson, L. M. and Damaske, D.: East Antarctic rifting  
1126 triggers uplift of the Gamburtsev Mountains, *Nature*, 479(7373), 388–392, 2011.
- 1127 Ferré, E. C., Friedman, S. A., Martín-Hernández, F., Feinberg, J. M., Conder, J. A. and Ionov, D. A.: The  
1128 magnetism of mantle xenoliths and potential implications for sub-Moho magnetic sources, *Geophysical Research  
1129 Letters*, 40(1), 105–110, 2013.

This page contains no comments



- 1130 Fisher, A. T. and Harris, R. N.: Using seafloor heat flow as a tracer to map subseafloor fluid flow in the ocean  
1131 crust, *Geofluids*, 10(1–2), 142–160, 2010.
- 1132 Fisher, A. T., Mankoff, K. D., Tulaczyk, S. M., Tyler, S. W., Foley, N. and others: High geothermal heat flux  
1133 measured below the West Antarctic Ice Sheet, *Science advances*, 1(6), e1500093, 2015.
- 1134 Flowerdew, M. J., Tyrrell, S., Boger, S. D., Fitzsimons, I. C. W., Harley, S. L., Mikhalsky, E. V. and Vaughan,  
1135 A. P. M.: Pb isotopic domains from the Indian Ocean sector of Antarctica: implications for past Antarctica–India  
1136 connections, *Geological Society, London, Special Publications*, 383(1), 59–72, 2013.
- 1137 Foster, T. D.: Temperature and salinity fields under the Ross Ice Shelf, *Antarctic Journal [of the United States]*,  
1138 13, 81–82, 1978.
- 1139 Fox Maule, C., Purucker, M. E., Olsen, N. and Mosegaard, K.: Heat flux anomalies in Antarctica revealed by  
1140 satellite magnetic data, *Science*, 309(5733), 464–467, 2005. 
- 1141 Fricker, H. A., Scambos, T., Bindshadler, R. and Padman, L.: An active subglacial water system in West  
1142 Antarctica mapped from space, *Science*, 315(5818), 1544–1548, 2007.
- 1143 Frost, B. R. and Shive, P. N.: Magnetic mineralogy of the lower continental-crust, *Journal of Geophysical  
1144 Research-Solid Earth and Planets*, 91(B6), 6513–6521, 1986.
- 1145 Fudge, T. J., Biyani, S., Clemens-Sewall, D. and Hawley, B.: Constraining geothermal flux at coastal domes of  
1146 the Ross Ice Sheet, Antarctica, *Geophysical Research Letters*, 2019.
- 1147 Gard, M., Hasterok, D. and Halpin, J. A.: Global whole-rock geochemical database compilation, *Earth System  
1148 Science Data*, 11(4), 1553–1566, doi:<https://doi.org/10.5194/essd-2019-50>, 2019.
- 1149 Godey, S., Deschamps, F., Trampert, J. and Snieder, R.: Thermal and compositional anomalies beneath the North  
1150 American continent, *Journal of Geophysical Research: Solid Earth*, 109(B1), 2004.
- 1151 Goelzer, H., Robinson, A., Seroussi, H. and Van De Wal, R. S.: Recent progress in Greenland ice sheet modelling,  
1152 *Current climate change reports*, 3(4), 291–302, 2017.
- 1153 Gohl, K., Wellner, J. S., Klaus, A. and Expedition 379 Scientists: Expedition 379 Preliminary Report: Amundsen  
1154 Sea West Antarctic Ice Sheet History, *International Ocean Discovery Program*, 379,  
1155 doi:<https://doi.org/10.14379/iodp.pr.379.2019>, 2019.
- 1156 Golynsky, A., Chiappini, M., Damaske, D., Ferraccioli, F., Finn, C. A., Ishihara, T., Kim, H. R., Kovacs, L.,  
1157 Masolov, V. N., Morris, P. and others: ADMAP—a digital magnetic anomaly map of the Antarctic, in *Antarctica*,  
1158 pp. 109–116, Springer., 2006.
- 1159 Goodge, J. W.: Crustal heat production and estimate of terrestrial heat flow in central East Antarctica, with  
1160 implications for thermal input to the East Antarctic ice sheet., *Cryosphere*, 12(2), 2018.
- 1161 Goodge, J. W. and Severinghaus, J. P.: Rapid Access Ice Drill: a new tool for exploration of the deep Antarctic  
1162 ice sheets and subglacial geology, *Journal of Glaciology*, 62(236), 1049–1064, 2016.
- 1163 Gow, A. J., Ueda, H. T. and Garfield, D. E.: Antarctic ice sheet: preliminary results of first core hole to bedrock,  
1164 *Science*, 161(3845), 1011–1013, 1968.
- 1165 Grauch, V. J. S.: Limitations on digital filtering of the DNAG magnetic data set for the conterminous US,  
1166 *Geophysics*, 58(9), 1281–1296, 1993.
- 1167 Greve, R. and Hutter, K.: Polythermal three-dimensional modelling of the Greenland ice sheet with varied  
1168 geothermal heat flux, *Annals of Glaciology*, 21(1), 8–12, 1995.
- 1169 Guimarães, S. N. P., Hamza, V. M. and Ravat, D.: Curie depths using combined analysis of centroid and matched  
1170 filtering methods in inferring thermomagnetic characteristics of Central Brazil, in *13th International Congress of*



Please also mention the updated version of this data set by Purucker 2013 which is the available data set now



- 1171 the Brazilian Geophysical Society & EXPOGEF, Rio de Janeiro, Brazil, 26–29 August 2013, pp. 1853–1858,  
 1172 Society of Exploration Geophysicists and Brazilian Geophysical Society., 2013.
- 1173 Gutenberg, B.: 6. Temperature and Thermal Processes in the Earth, in *International Geophysics*, vol. 1, edited by  
 1174 B. Gutenberg, pp. 121–148, Academic Press Inc., New York., 1959.
- 1175 Haggerty, S. E.: Mineralogical constraints on Curie isotherms in deep crustal magnetic anomalies, *Geophysical*  
 1176 *Research Letters*, 5(2), 105–108, 1978.
- 1177 Halpin, J. A. and Reading, A. M.: Report on Taking the Temperature of the Antarctic Continent (TACtical)  
 1178 Workshop 21–23 March 2018, Hobart, Tasmania, Australia, Hobart, Australia., 2018.
- 1179 Halpin, J. A., Whittaker, J. M., Gard, M., Hasterok, D., Burton-Johnson, A., Staal, T., Maritati, A., Reading, A.  
 1180 M., McLaren, S., Hand, M. and Raimondo, T.: Heterogenous Antarctic crustal heat production, Incheon, Republic  
 1181 of Korea., 2019.
- 1182 Han, U. and Chapman, D. S.: Thermal isostasy: Elevation change of geologic provinces, *Journal of the Geological*  
 1183 *Society of Korea*, 31(2), 106–115, 1995.
- 1184 Hasterok, D. and Chapman, D. S.: Continental thermal isostasy: 1. Methods and sensitivity, *Journal of*  
 1185 *Geophysical Research: Solid Earth*, 112(B6), 2007a.
- 1186 Hasterok, D. and Chapman, D. S.: Continental thermal isostasy: 2. Application to North America, *Journal of*  
 1187 *Geophysical Research: Solid Earth*, 112(B6), 2007b.
- 1188 Hasterok, D. and Chapman, D. S.: Heat production and geotherms for the continental lithosphere, *Earth and*  
 1189 *Planetary Science Letters*, 307(1–2), 59–70, doi:10.1016/j.epsl.2011.04.034, 2011.
- 1190 Hasterok, D. and Gard, M.: Utilizing thermal isostasy to estimate sub-lithospheric heat flow and anomalous crustal  
 1191 radioactivity, *Earth and Planetary Science Letters*, 450, 197–207, 2016.
- 1192 Hasterok, D., Gard, M., Halpin, J. A., Hand, M. P., Pollett, A., McLaren, S., Raimondo, T., Willcocks, S. and  
 1193 Linke, M.: Constraining Geothermal Heat Flux Beneath Ice Sheets Using Thermal Isostasy, in *AGU Fall Meeting*  
 1194 *2019, AGU.*, 2019.
- 1195 Hillenbrand, C.-D., Smith, J. A., Hodell, D. A., Greaves, M., Poole, C. R., Kender, S., Williams, M., Andersen,  
 1196 T. J., Jernas, P. E. and Elderfield, H.: West Antarctic Ice Sheet retreat driven by Holocene warm water incursions,  
 1197 *Nature*, 547(7661), 43, 2017.
- 1198 Hindmarsh, R. C. and Ritz, C. M.: How deep do you need to drill through ice to measure the geothermal heat  
 1199 flux?, in *EGU General Assembly Conference Abstracts*, vol. 14, p. 8629., 2012.
- 1200 Hondoh, T., Shoji, H., Watanabe, O., Salamatin, A. N. and Lipenkov, V. Y.: Depth–age and temperature  
 1201 prediction at Dome Fuji station, East Antarctica, *Annals of Glaciology*, 35, 384–390, 2002.
- 1202 Huang, Y., Chubakov, V., Mantovani, F., Rudnick, R. L. and McDonough, W. F.: A reference Earth model for  
 1203 the heat-producing elements and associated geoneutrino flux, *Geochemistry, Geophysics, Geosystems*, 14(6),  
 1204 2003–2029, 2013.
- 1205 Hughes, T.: Modeling ice sheets from the bottom up, *Quaternary Science Reviews*, 28(19–20), 1831–1849, 2009.
- 1206 Hyvönen, E., Turunen, P., Vanhanen, E., Arkimaa, H. and Sutinen, R.: Airborne gamma-ray surveys in Finland,  
 1207 *Aerogeophysics in Finland*, 2004, 1972.
- 1208 Jaeger, J. C.: Numerical values for the temperature in radial heat flow, *Journal of Mathematics and Physics*, 34(1–  
 1209 4), 316–321, 1956.
- 1210 Jaeger, J. C.: The effect of the drilling fluid on temperatures measured in bore holes, *Journal of Geophysical*  
 1211 *Research*, 66(2), 563–569, 1961.





- 1212 Jaeger, J. C.: Application of the theory of heat conduction to geothermal measurements, *Terrestrial heat flow*, 8,  
1213 7–23, 1965.
- 1214 James, D. W.: The thermal diffusivity of ice and water between- 40 and+ 60° C, *Journal of Materials Science*,  
1215 3(5), 540–543, 1968.
- 1216 Jezek, K. C., Johnson, J. T., Drinkwater, M. R., Macelloni, G., Tsang, L., Aksoy, M. and Durand, M.: Radiometric  
1217 approach for estimating relative changes in intraglacier average temperature, *IEEE Transactions on Geoscience*  
1218 *and Remote Sensing*, 53(1), 134–143, 2014.
- 1219 Jordan, T., Martin, C., Ferraccioli, F., Matsuoka, K., Corr, H., Forsberg, R., Olesen, A. and Siegert, M. J.: Newly  
1220 discovered geothermal anomaly at South Pole ice divide; origins and implications, in *Geophysical Research*  
1221 *Abstracts*, vol. 20, p. 15511., 2018.
- 1222 Jordan, T. A., Riley, T. R. and Siddoway, C. S.: The geological history and evolution of West Antarctica, *Nature*  
1223 *Reviews Earth & Environment*, 1, 117–133, 2020.
- 1224 Kawakatsu, H. and Watada, S.: Seismic evidence for deep-water transportation in the mantle, *Science*, 316(5830),  
1225 1468–1471, 2007.
- 1226 Kerr, Y. H., Waldteufel, P., Wigneron, J.-P., Delwart, S., Cabot, F., Boutin, J., Escorihuela, M.-J., Font, J., Reul,  
1227 N. and Gruhier, C.: The SMOS mission: New tool for monitoring key elements of the global water cycle,  
1228 *Proceedings of the IEEE*, 98(5), 666–687, 2010.
- 1229 Kingslake, J., Scherer, R. P., Albrecht, T., Coenen, J., Powell, R. D., Reese, R., Stansell, N. D., Tulaczyk, S.,  
1230 Wearing, M. G. and Whitehouse, P. L.: Extensive retreat and re-advance of the West Antarctic Ice Sheet during  
1231 the Holocene, *Nature*, 558(7710), 430–434, 2018.
- 1232 Korenaga, J.: Earth’s heat budget: Clairvoyant geoneutrinos, *Nature Geoscience*, 4(9), 581, 2011.
- 1233 Kuchar, J. and Milne, G. A.: The influence of viscosity structure in the lithosphere on predictions from models of  
1234 glacial isostatic adjustment, *Journal of Geodynamics*, 86, 1–9, 2015.
- 1235 Lachenbruch, A. H.: Preliminary geothermal model of the Sierra Nevada, *Journal of Geophysical Research*,  
1236 73(22), 6977–6989, 1968.
- 1237 Lachenbruch, A. H.: Crustal temperature and heat production: Implications of the linear heat-flow relation, *Journal*  
1238 *of Geophysical Research*, 75(17), 3291–3300, 1970.
- 1239 Lachenbruch, A. H. and Brewer, M. C.: Dissipation of the temperature effect of drilling a well in Arctic Alaska,  
1240 *United States Geological Survey Bulletin*, 1083–C, 73–109, 1959.
- 1241 Langel, R. A. and Hinze, W. J.: *The magnetic field of the Earth’s lithosphere: The satellite perspective*, Cambridge  
1242 University Press, Cambridge, UK., 1998.
- 1243 Larour, E., Morlighem, M., Seroussi, H., Schiermeier, J. and Rignot, E.: Ice flow sensitivity to geothermal heat  
1244 flux of Pine Island Glacier, Antarctica, *Journal of Geophysical Research: Earth Surface*, 117(F4), 2012.
- 1245 Leat, P. T., Jordan, T. A., Flowerdew, M. J., Riley, T. R., Ferraccioli, F. and Whitehouse, M. J.: Jurassic high heat  
1246 production granites associated with the Weddell Sea rift system, Antarctica, *Tectonophysics*, 722, 249–264, 2018.
- 1247 Lees, C. H.: On the shapes of the isogeotherms under mountain ranges in radio-active districts, *Proceedings of the*  
1248 *Royal Society of London. Series A, Containing Papers of a Mathematical and Physical Character*, 83(563), 339–  
1249 346, 1910.
- 1250 Li, C.-F., Lu, Y. and Wang, J.: A global reference model of Curie-point depths based on EMAG2, *Scientific*  
1251 *reports*, 7, 45129, 2017.

This page contains no comments





- 1252 Jefferinge, B. V. and Pattyn, F.: Using ice-flow models to evaluate potential sites of million year-old ice in  
1253 Antarctica, *Climate of the Past*, 9(5), 2335–2345, 2013.
- 1254 Jefferinge, B. V., Pattyn, F., Cavitte, M. G., Karlsson, N. B., Young, D. A., Sutter, J. and Eisen, O.: Promising  
1255 West Ice sites in East Antarctica based on thermodynamical modelling, *The Cryosphere*, 12(8), 2773–2787,  
1256 2018.
- 1257 Llubes, M., Lanseau, C. and Rémy, F.: Relations between basal condition, subglacial hydrological networks and  
1258 geothermal flux in Antarctica, *Earth and Planetary Science Letters*, 241(3), 655–662, 2006.
- 1259 Lowrie, W.: *Fundamentals of geophysics*, 2nd ed., Cambridge University Press, Cambridge., 2007.
- 1260 Lucazeau, F.: Analysis and mapping of an updated terrestrial heat flow dataset, *Geochemistry, Geophysics,*  
1261 *Geosystems*, 2019.
- 1262 Macelloni, G., Leduc-Leballeur, M., Brogioni, M., Ritz, C. and Picard, G.: Analyzing and modeling the SMOS  
1263 spatial variations in the East Antarctic Plateau, *Remote sensing of environment*, 180, 193–204, 2016.
- 1264 Macelloni, G., Brogioni, M., Leduc-Leballeur, M., Montomoli, F., Bartsch, A., Mialon, A., Ritz, C., Soteras, J.  
1265 C., Stammer, D. and Picard, G.: Cryorad: A Low Frequency Wideband Radiometer Mission for the Study of the  
1266 Cryosphere, in *IGARSS 2018-2018 IEEE International Geoscience and Remote Sensing Symposium*, pp. 1998–  
1267 2000, IEEE., 2018.
- 1268 Macelloni, G., Leduc-Leballeur, M., Montomoli, F., Brogioni, M., Ritz, C. and Picard, G.: On the retrieval of  
1269 internal temperature of Antarctica Ice Sheet by using SMOS observations, *Remote Sensing of Environment*, 233,  
1270 111405, 2019.
- 1271 Mareschal, J. C. and Jaupart, C.: Radiogenic heat production, thermal regime and evolution of continental crust,  
1272 *Tectonophysics*, 609, 524–534, doi:10.1016/j.tecto.2012.12.001, 2013.
- 1273 Martin, A. P. and van der Wal, W., Eds.: *The Antarctic Mantle*, The Geological Society, London, UK., in prep.
- 1274 Martin, A. P., Cooper, A. F. and Price, R. C.: Increased mantle heat flow with on-going rifting of the West  
1275 Antarctic rift system inferred from characterisation of plagioclase peridotite in the shallow Antarctic mantle,  
1276 *Lithos*, 190, 173–190, 2014.
- 1277 Martos, Y. M., Catalán, M., Jordan, T. A., Golynsky, A., Golynsky, D., Eagles, G. and Vaughan, D. G.: Heat flux  
1278 distribution of Antarctica unveiled, *Geophysical Research Letters*, 44(22), 11–417, 2017.
- 1279 Martos, Y. M., Jordan, T. A., Catalán, M., Jordan, T. M., Bamber, J. L. and Vaughan, D. G.: Geothermal heat flux  
1280 reveals the Iceland hotspot track underneath Greenland, *Geophysical Research Letters*, 45(16), 8214–8222, 2018.
- 1281 Maus, S.: Magnetic field model MF7. Retrieved August 28, 2018, from [www.geomag.us/models/MF7.html](http://www.geomag.us/models/MF7.html),  
1282 2010.
- 1283 Mayhew, M. A.: Inversion of satellite magnetic anomaly data, *Journal of Geophysics*, 45(1), 119–128, 1979.
- 1284 McDonough, W. F. and Sun, S. s.: The composition of the Earth, *Chemical Geology*, 120(3–4), 223–253,  
1285 doi:10.1016/0009-2541(94)00140-4, 1995.
- 1286 McKay, R., De Santis, L., Kulhanek, D. K. and Expedition 374 Scientists: International Ocean Discovery Program  
1287 Expedition 374 Preliminary Report: Ross Sea West Antarctic Ice Sheet History, International Ocean Discovery  
1288 Program, 374, doi:<https://doi.org/10.14379/iodp.pr.374.2018>, 2018.
- 1289 McKenzie, D., Jackson, J. and Priestley, K.: Thermal structure of oceanic and continental lithosphere, *Earth and*  
1290 *Planetary Science Letters*, 233(3–4), 337–349, 2005.



---

Number: 1	Author: brice	Subject: Highlight	Date: 13/04/2020 10:30:46
-----------	---------------	--------------------	---------------------------

---

Van Liefferinge, B., and Pattyn, F.: ...



---

Number: 2	Author: brice	Subject: Inserted Text	Date: 13/04/2020 10:31:15
-----------	---------------	------------------------	---------------------------

---

Van



- 1291 de Mendoza, I. H., Mareschal, J.-C. and Beltrami, H.: Constraints on glacier flow from temperature-depth profiles  
 1292 in the ice. Application to EPICA Dome C., *Climate of the Past Discussions*, doi:https://doi.org/10.5194/cp-2016-  
 1293 116, 2016.
- 1294 Morgan, J. P., Rüpke, L. H. and White, W. M.: The Current Energetics of Earth's Interior: A Gravitational Energy  
 1295 Perspective, *Frontiers in Earth Science*, 4(May), 1–28, doi:10.3389/feart.2016.00046, 2016.
- 1296 Morin, R. H., Williams, T., Henrys, S. A., Magens, D., Niessen, F. and Hansaraj, D.: Heat flow and hydrologic  
 1297 characteristics at the AND-1B borehole, ANDRILL McMurdo Ice Shelf Project, Antarctica, *Geosphere*, 6(4),  
 1298 370–378, 2010.
- 1299 Mulder, J. A., Halpin, J. A., Daczko, N. R., Orth, K., Meffre, S., Thompson, J. M. and Morrissey, L. J.: A  
 1300 Multiproxy provenance approach to uncovering the assembly of East Gondwana in Antarctica, *Geology*, 47(7),  
 1301 645–649, 2019.
- 1302 Müller, C., Usbeck, R. and Miesner, F.: Temperatures in shallow marine sediments: Influence of thermal  
 1303 properties, seasonal forcing, and man-made heat sources, *Applied Thermal Engineering*, 108, 20–29, 2016.
- 1304 Mulvaney, R., Abram, N. J., Hindmarsh, R. C., Arrowsmith, C., Fleet, L., Triest, J., Sime, L. C., Alemany, O. and  
 1305 Foord, S.: Recent Antarctic Peninsula warming relative to Holocene climate and ice-shelf history, *Nature*,  
 1306 489(7414), 141–144, 2012.
- 1307 Mulvaney, R., Martin, C., Massam, A., Rix, J. and Ritz, C.: Estimating geothermal heat flux from ice sheet  
 1308 borehole temperature measurements, in *XIII International Symposium on Antarctic Earth Sciences*, Incheon,  
 1309 Republic of Korea., 2019.
- 1310 Nicholls, K. W. and Paren, J. G.: Extending the Antarctic meteorological record using ice-sheet temperature  
 1311 profiles, *Journal of climate*, 6(1), 141–150, 1993.
- 1312 Obande, G. E., Lawal, K. M. and Ahmed, L. A.: Spectral analysis of aeromagnetic data for geothermal  
 1313 investigation of Wikki Warm Spring, north-east Nigeria, *Geothermics*, 50, 85–90, 2014.
- 1314 Okubo, Y., Graf, R. J., Hansen, R. O., Ogawa, K. and Tsu, H.: Curie point depths of the island of Kyushu and  
 1315 surrounding areas, Japan, *Geophysics*, 50(3), 481–494, 1985.
- 1316 Olesen, O., Balling, N., Barrère, C., Breiner, N., Davidsen, B., Ebbing, J., Elvebakk, H., Gernigon, L., Koziel, J.,  
 1317 Lutro, O. and others: KONTIKI final report, continental crust and heat generation in 3D, NGU Report, 42, 2007.
- 1318 Pappa, F., Ebbing, J., Ferraccioli, F. and van der Wal, W.: Modeling satellite gravity gradient data to derive  
 1319 density, temperature, and viscosity structure of the Antarctic lithosphere, *Journal of Geophysical Research: Solid*  
 1320 *Earth*, 124, 12053–12076, 2019a.
- 1321 Pappa, F., Ebbing, J. and Ferraccioli, F.: Moho Depths of Antarctica: Comparison of Seismic, Gravity, and  
 1322 Isostatic Results, *Geochemistry, Geophysics, Geosystems*, 20, 2019b.
- 1323 Passalacqua, O., Ritz, C., Parrenin, F., Urbini, S. and Frezzotti, M.: Geothermal flux and basal melt rate in the  
 1324 Dome C region inferred from radar reflectivity and heat modelling, *The Cryosphere*, 2017.
- 1325 Passalacqua, O., Picard, G., Ritz, C., Leduc-Leballeur, M., Quiquet, A., Larue, F. and Macelloni, G.: Retrieval of  
 1326 the Absorption Coefficient of L-Band Radiation in Antarctica From SMOS Observations, *Remote Sensing*,  
 1327 10(12), 1954, 2018.
- 1328 Paterson, W. S. B.: *The physics of glaciers*, Third Edition., Elsevier, Oxford, UK., 1994.
- 1329 Pattyn, F.: Antarctic subglacial conditions inferred from a hybrid ice sheet/ice stream model, *Earth and Planetary*  
 1330 *Science Letters*, 295(3), 451–461, 2010.
- 1331 Pfender, M. and Villinger, H.: Miniaturized data loggers for deep sea sediment temperature gradient  
 1332 measurements, *Marine Geology*, 186(3–4), 557–570, 2002.

This page contains no comments



- 1333 Phaneuf, C. and Mareschal, J.-C.: Estimating concentrations of heat producing elements in the crust near the  
1334 Sudbury Neutrino Observatory, Ontario, Canada, *Tectonophysics*, 622, 135–144, 2014.
- 1335 Pittard, M. L., Galton-Fenzi, B. K., Roberts, J. L. and Watson, C. S.: Organization of ice flow by localized regions  
1336 of elevated geothermal heat flux, *Geophysical Research Letters*, 43(7), 3342–3350, 2016a.
- 1337 Pittard, M. L., Roberts, J. L., Galton-Fenzi, B. K. and Watson, C. S.: Sensitivity of the Lambert-Amery glacial  
1338 system to geothermal heat flux, *Annals of Glaciology*, 57(73), 56–68, 2016b.
- 1339 Pollack, H. N. and Chapman, D. S.: Mantle heat flow, *Earth and Planetary Science Letters*, 34(2), 174–184, 1977.
- 1340 Pollack, H. N., Hurter, S. J. and Johnson, J. R.: Heat flow from the Earth's interior: Analysis of the global data  
1341 set, *Reviews of Geophysics*, 31(3), 267–280, doi:10.1029/93RG01249, 1993.
- 1342 Pollard, D., DeConto, R. M. and Nyblade, A. A.: Sensitivity of Cenozoic Antarctic ice sheet variations to  
1343 geothermal heat flux, *Global and Planetary Change*, 49(1), 63–74, 2005.
- 1344 Pollett, A., Hasterok, D., Raimondo, T., Halpin, J. A., Hand, M., Bendall, B. and McLaren, S.: Heat flow in  
1345 southern Australia and connections with East Antarctica, *Geochemistry, Geophysics, Geosystems*, 2019.
- 1346 Popov, Y. A., Pevzner, S. L., Pimenov, V. P. and Romushkevich, R. A.: New geothermal data from the Kola  
1347 superdeep well SG-3, *Tectonophysics*, 306(3–4), 345–366, 1999.
- 1348 Price, P. B., Nagornov, O. V., Bay, R., Chirkin, D., He, Y., Miocinovic, P., Richards, A., Woschnagg, K., Koci,  
1349 B. and Zagorodnov, V.: Temperature profile for glacial ice at the South Pole: Implications for life in a nearby  
1350 subglacial lake, *Proceedings of the National Academy of Sciences*, 99(12), 7844–7847, 2002.
- 1351 Pruss, E. F., Decker, E. R. and Smithson, S. B.: Preliminary temperature-measurements at DVDP holes 3, 4, 6,  
1352 and 8, *Antarctic Journal of the United States*, 9(4), 133–134, 1974.
- 1353 Purucker, M. and Whaler, K.: Crustal magnetism, edited by M. Kono, *Treatise on Geophysics*, 5, 195–237, 2007.
- 1354 Ravat, D., Pignatelli, A., Nicolosi, I. and Chiappini, M.: A study of spectral methods of estimating the depth to  
1355 the bottom of magnetic sources from near-surface magnetic anomaly data, *Geophysical Journal International*,  
1356 169(2), 421–434, 2007.
- 1357 Rémy, F. and Legresy, B.: Subglacial hydrological networks in Antarctica and their impact on ice flow, *Annals  
1358 of Glaciology*, 39, 67–72, 2004.
- 1359 Risk, G. F. and Hochstein, M. P.: Heat flow at arrival heights, Ross Island, Antarctica, *New Zealand Journal of  
1360 Geology and Geophysics*, 17(3), 629–644, 1974.
- 1361 Ritz, C.: Time dependent boundary conditions for calculation of temperature fields in ice sheets, in *The Physical  
1362 Basis of Ice Sheet Modelling (Proceedings of the Vancouver Symposium, August 1987)*, vol. IAHS Publ. no. 170,  
1363 pp. 207–216, Vancouver, Canada., 1987.
- 1364 Ritz, C.: Interpretation of the temperature profile measured at Vostok, East Antarctica, *Annals of glaciology*, 12,  
1365 138–144, 1989.
- 1366 Rix, J., Mulvaney, R., Hong, J. and Ashurst, D.: Development of the British Antarctic Survey Rapid Access  
1367 Isotope Drill, *Journal of Glaciology*, 65(250), 288–298, 2019.
- 1368 Rogozhina, I., Hagedoorn, J. M., Martinec, Z., Fleming, K., Soucek, O., Greve, R. and Thomas, M.: Effects of  
1369 uncertainties in the geothermal heat flux distribution on the Greenland Ice Sheet: An assessment of existing heat  
1370 flow models, *Journal of Geophysical Research: Earth Surface*, 117, F02025, doi:doi:10.1029/2011JF002098,  
1371 2012.
- 1372 Ross, H. E., Blakely, R. J. and Zoback, M. D.: Testing the use of aeromagnetic data for the determination of Curie  
1373 depth in California, *Geophysics*, 71(5), L51–L59, 2006.

This page contains no comments



- 1374 Roy, R. F., Blackwell, D. D. and Birch, F.: Heat generation of plutonic rocks and continental heat flow provinces,  
 1375 Earth and Planetary Science Letters, 5, 1–12, 1968.
- 1376 Rudnick, R. and Fountain, D.: Nature and composition of the continental crust: a lower crustal perspective,  
 1377 Reviews of Geophysics, (95), 267–309, 1995.
- 1378 Rudnick, R. L., McDonough, W. F. and O'Connell, R. J.: Thermal structure, thickness and composition of  
 1379 continental lithosphere, Chemical Geology, 145(3–4), 395–411, 1998.
- 1380 Rybach, L.: Amount and significance of radioactive heat sources in sediments, Collection colloques seminaires,  
 1381 44, 311–322, 1986.
- 1382 Salamatin, A. N., Lipenkov, V. Y., Barkov, N. I., Jouzel, J., Petit, J. R. and Raynaud, D.: Ice core age dating and  
 1383 paleothermometer calibration based on isotope and temperature profiles from deep boreholes at Vostok Station  
 1384 (East Antarctica), Journal of Geophysical Research: Atmospheres, 103(D8), 8963–8977, 1998.
- 1385 Salem, A., Green, C., Ravat, D., Singh, K. H., East, P., Fairhead, J. D., Mogren, S. and Biegert, E.: Depth to Curie  
 1386 temperature across the central Red Sea from magnetic data using the de-fractal method, Tectonophysics, 624, 75–  
 1387 86, 2014.
- 1388 Sandiford, M. and Hand, M.: Controls on the locus of intraplate deformation in central Australia, Earth and  
 1389 Planetary Science Letters, 162(1–4), 97–110, 1998.
- 1390 Sandiford, M. and McLaren, S.: Tectonic feedback and the ordering of heat producing elements within the  
 1391 continental lithosphere, Earth and Planetary Science Letters, 204(1), 133–150, 2002.
- 1392 Schroeder, D. M., Blankenship, D. D., Young, D. A. and Quartini, E.: Evidence for elevated and spatially variable  
 1393 geothermal flux beneath the West Antarctic Ice Sheet, Proceedings of the National Academy of Sciences, 111(25),  
 1394 9070–9072, 2014.
- 1395 Sclater, J., Jaupart, C. and Galson, D.: The heat flow through oceanic and continental crust and the heat loss of  
 1396 the Earth, Reviews of Geophysics, 18(1), 269–311, 1980.
- 1397 Shapiro, N. M. and Ritzwoller, M. H.: Monte-Carlo inversion for a global shear-velocity model of the crust and  
 1398 upper mantle, Geophysical Journal International, 151(1), 88–105, 2002.
- 1399 Shapiro, N. M. and Ritzwoller, M. H.: Inferring surface heat flux distributions guided by a global seismic model:  
 1400 particular application to Antarctica, Earth and Planetary Science Letters, 223(1), 213–224, 2004.
- 1401 Siegert, M. J.: Antarctic subglacial lakes, Earth-Science Reviews, 50(1), 29–50, 2000.
- 1402 Siegert, M. J. and Dowdeswell, J. A.: Spatial variations in heat at the base of the Antarctic ice sheet from analysis  
 1403 of the thermal regime above subglacial lakes, Journal of Glaciology, 42(142), 501–509, 1996.
- 1404 Slagstad, T.: Radiogenic heat production of Archaean to Permian geological provinces in Norway., Norwegian  
 1405 Journal of Geology/Norsk Geologisk Forening, 88(3), 2008.
- 1406 Spector, A. and Grant, F. S.: Statistical models for interpreting aeromagnetic data, Geophysics, 35(2), 293–302,  
 1407 1970.
- 1408 Stein, C. A. and Stein, S.: A model for the global variation in oceanic depth and heat flow with lithospheric age,  
 1409 Nature, 359(6391), 123, 1992.
- 1410 Stein, C. A. and Stein, S.: Mantle plumes: heat-flow near Iceland, Astronomy & Geophysics, 44(1), 1–8, 2003.
- 1411 Swanberg, C. A.: Vertical distribution of heat generation in the Idaho batholith, Journal of Geophysical Research,  
 1412 77(14), 2508–2513, 1972.

This page contains no comments





- 1413 Talalay, P. G. and Pyne, A. R.: Geological drilling in McMurdo Dry Valleys and McMurdo Sound, Antarctica:  
1414 Historical development, *Cold Regions Science and Technology*, 141, 131–162, 2017.
- 1415 Tanaka, A., Okubo, Y. and Matsubayashi, O.: Curie point depth based on spectrum analysis of the magnetic  
1416 anomaly data in East and Southeast Asia, *Tectonophysics*, 306(3–4), 461–470, 1999.
- 1417 Taylor, S. R. and McLennan, S. M.: The continental crust: its composition and evolution, [online] Available from:  
1418 <http://www.osti.gov/scitech/biblio/6582885> (Accessed 7 March 2017), 1985.
- 1419 Trifonova, P., Zhelev, Z., Petrova, T. and Bojadgieva, K.: Curie point depths of Bulgarian territory inferred from  
1420 geomagnetic observations and its correlation with regional thermal structure and seismicity, *Tectonophysics*,  
1421 473(3–4), 362–374, 2009.
- 1422 Turcotte, D. L. and Schubert, G.: *Geodynamics*, Cambridge University Press, Cambridge, UK., 2014.
- 1423 Veikkolainen, T. and Kukkonen, I. T.: Highly varying radiogenic heat production in Finland, Fennoscandian  
1424 Shield, *Tectonophysics*, 750, 93–116, 2019.
- 1425 Vieli, G.-M. L., Martin, C., Hindmarsh, R. C. A. and Lüthi, M. P.: Basal freeze-on generates complex ice-sheet  
1426 stratigraphy, *Nature communications*, 9(1), 1–13, 2018.
- 1427 Vitorello, I. and Pollack, H. N.: On the variation of continental heat flow with age and the thermal evolution of  
1428 continents, *Journal of Geophysical Research: Solid Earth*, 85(B2), 983–995, 1980.
- 1429 Vosteen, H.-D. and Schellschmidt, R.: Influence of temperature on thermal conductivity, thermal capacity and  
1430 thermal diffusivity for different types of rock, *Physics and Chemistry of the Earth, Parts A/B/C*, 28(9–11), 499–  
1431 509, 2003.
- 1432 van der Wal, W., Barnhoorn, A., Stocchi, P., Gradmann, S., Wu, P., Drury, M. and Vermeersen, B.: Glacial  
1433 isostatic adjustment model with composite 3-D Earth rheology for Fennoscandia, *Geophysical Journal  
1434 International*, 194(1), 61–77, 2013.
- 1435 van der Wal, W., Whitehouse, P. L. and Schrama, E. J.: Effect of GIA models with 3D composite mantle viscosity  
1436 on GRACE mass balance estimates for Antarctica, *Earth and Planetary Science Letters*, 414, 134–143, 2015.
- 1437 Wangen, M.: *Physical principles of sedimentary basin analysis*, Cambridge University Press, Cambridge, UK.,  
1438 2010.
- 1439 Wasilewski, P. J. and Mayhew, M. A.: The Moho as a magnetic boundary revisited, *Geophysical Research Letters*,  
1440 19(22), 2259–2262, 1992.
- 1441 Winsborrow, M. C., Clark, C. D. and Stokes, C. R.: What controls the location of ice streams?, *Earth-Science  
1442 Reviews*, 103(1), 45–59, 2010.
- 1443 Wright, A. and Siegert, M.: A fourth inventory of Antarctic subglacial lakes, *Antarctic Science*, 24(6), 659–664,  
1444 2012.
- 1445 Zagorodnov, V., Nagornov, O., Scambos, T. A., Muto, A., Mosley-Thompson, E., Pettit, E. C. and Tyufin, S.:  
1446 Borehole temperatures reveal details of 20th century warming at Bruce Plateau, Antarctic Peninsula, *The  
1447 Cryosphere*, 6(3), 675–686, 2012.
- 1448

This page contains no comments